SIMULATIONS AND SILICON WAFER COMPATIBILITY OF A
VOLTAGE-CONTROLLED OPTICAL SWITCH USING ITO/NbOx

By

Kevin Burghardt

A THESIS

Submitted to
Michigan State University
in partial fulfillments
for the degree of

Electrical Engineering - Master of Science

2017

ABSTRACT

**SIMULATIONS AND SILICON WAFER COMPATIBILITY OF A
VOLTAGE-CONTROLLED OPTICAL SWITCH USING ITO/NbOx**

By

Kevin Burghardt

The story of optics and processing has always been on of silicon devices making strides faster and cheaper than optics. The idea of creating optical switches has been generally relegated to academic exercises or niche markets. This research takes a view of optical processing that is complimentary to silicon. Silicon wafers produce extremely dense, high quality devices but producing truly 3D integrated circuits has been a challenge. It would be advantageous to not need to bond wafers to create a 3D active structure. An argument for an optical switch that has a simple structure and uses industry established fabrication methods is given. The proposed switch uses the material indium tin oxide nanoparticles in niobum oxide glass (ITO/NbO$_x$) as the active layer. The transmittance through this material is proportional to the electric field applied to it meaning the structure of a capacitor could be used to control it. It uses a metal for one plate of the capacitor and the ITO/NbO$_x$ as the other plate with the light running through ITO/NbO$_x$ plate. Each of the plates are separated from one another and surrounded by a dielectric material. Simulations show that silicon dioxide (SiO$_2$) can be used effectively to turn the ITO/NbO$_x$ into a light guide with a transmittance controllable using an applied voltage and that the proposed structure can be created using industry established wafer fabrication processes.

TABLE OF CONTENTS

LIST OF TABLES

LIST OF FIGURES

INTRODUCTION

The fields of electronics and optics have had an increasing level of combined interested over the years. Starting with things like LEDs, photo sensors, and fiber optics there has been more and more interest in looking at the two as one. From an industry perspective, the focus has been finding an all optical switching solution for fiber optic networks. Currently these systems generally are required to go optical-electrical-optical in order to perform things like AB switching operations [1]. To this end, the commercial focus for Silicon-based chips is geared specifically towards optical switching. While there have been attempts at optical processors nothing has been made commercially available [2]. The main reason for this is Silicon processes are well understood and the cost of creating devices with this material is low enough that it is very difficult for devices based off of other materials to compete. Additionally, device density can be pushed very small with the theoretical limit of Silicon-based transistors down in the 10nm to 20nm range for gate width [3]. One drawback to Silicon-based MOSFET technology is the RC constant associated with the gate capacitance and the necessity of moving that charge from one part of a circuit to another. There is a physical limit to both how fast the fields can be created in the channel region and to how fast the electrons can be moved onto and off of the gate effectively limiting switching speed. While using photons in place of electrons will not result in moving the particles at the absolute speed limit of light because they will be traveling through a medium, it may be possible to push processing speeds faster. Moving directly to photon only based technology would be a massive undertaking; however with recent advancements in materials, developing a hybrid electron-photon device may be possible. The exact interaction between the electrons and photons would be dependent on the material. Vanadium dioxide, for example, requires heating and cooling to transition optical states so electrons would need to be able to manage localized temperatures. This could be done through something as simple as ohmic heating or as complicated as an LED that converts limited amounts of heat to light [4]. Another example, indium tin oxide (ITO) in niobium oxide glass (NbO_x), could potentially be controlled using the accumulation of charge similar to a traditional MOSFET [5]. Each different method has pros and cons associated with its specific electron-photon interaction. This approach represents an intermediary step between electron-based logic and photon-

based logic. The ultimate goal is system and fabrication process that will be simple enough to allow for a relatively fast research to fabrication cycle allowing for greater flexibility in experimentation.

For logic or processing applications an electron-controlled photon switch would be needed. Optical switching is once again an area where the focus on research has been on communications. The goal of that research is the ability to keep all signals optical in a network. The existing ideas for optical switching consists of AB or array switches. These types of switches require that light changes directions often through changing the index of refraction of a material that the light passes through. The advantage to this method is there usually aren't any moving parts. Conversely, something like a micro-mirror requires mechanical movement [1]. Even the original optical processor relies on a liquid crystal cell to effect the phase of the light resulting in either constructive or destructive interference [2]. Finding a way to create a light switch that uses existing fabrication techniques could be very advantageous in that it could allow for the creation of 3D structures or multiple layers of active structures that are simpler to make and design. The problem with the more traditional methods of switching is the reliance on changing the direction that light travels. Once feature sizes get small enough, things like edge effects and diffraction effectively start canceling out this change in direction. The direction of propagation may be changing but the light is spreading out enough that any sensor would still be illuminated. For this reason an absorptive switching scheme is being considered. In this scheme, light is either blocked or allowed to pass. This could be thought of as a fiber optic cable in which the core material could be turned "on" or "off" allowing light to pass or be absorbed respectively. Using this method should allow structures to get smaller than the switches that rely on light redirection.   The trade-off is that diffraction and the edge effects become very large compared to the light guide's cross-sectional dimensions become smaller than the light's wavelength. The challenge then becomes managing these effects such that adjacent light guides are not affected by cross-talk.

CHAPTER 1 LITERATURE REVIEW

Optical Processing

The subject of optics and processing has periodically made its way into articles as Silicon-based semiconductors have met their periodic roadblocks as the industry has been scaling the technology down. Prior to that, optics had a fairly rich period of research when the relative superiority of semiconductors was less certain. This period of research and its subsequent evolution is detailed extensively in an *Advances in Optical Technologies* article called "Optical Computing: A 60 Year Adventure" [6]. The article discusses how the focus of optics and information processing has changed from the goal of all optical to viewing it as a compliment to Silicon-based semiconductors. One of the early goals was to develop methods of taking advantage of the parallel processing potential of optics. This is a goal which has never really gone away. Even today there is a company in United Kingdom called Optalysys which is researching using Fourier transforms for parallel processing with analog light signals [7]. While parallel processing using light seems to be getting looked at again, advancements have been made using Silicon-based CMOS designs in quantum computing which also claim parallel processing capabilities [8, 9]. This is indicative of the historical relationship between optics and Silicon. As it seems the field of optics starts making some progress, Silicon makes a comparable advancement and is able to do so at either a smaller scale or cheaper cost. In this case, potentially developing parallel processing utilizing existing fabrication methods would be a huge advantage over anything in the optics field. Where optics has made a major impact on information processing is in digital communications [6]. Fiber optics has largely enabled the revolution in connectivity and information sharing that has defined beginning of the 21st century. Fiber optics provide a low loss high data density method for transmitting information over long distances. Demands for faster speeds have persisted highlighting the challenges to the interface between optics and electronics. It is here where much of the research in optics related information processing has focused for the last twenty or so years.

Optical processing can take place in an analog form often using some sort of planar parallel processing or in digital form which can be thought of as more analogous to serial processing. In traditional digital

processing there is true serial processing like communications and traditional multibit processing like in microprocessors and microcontrollers. While microprocessors and microcontrollers process multiple bits during each clock cycle a planar parallel system can process multiple microprocessors with each clock cycle representing another order of parallelism. For example a 64-bit system can process one 64 bit operation representing 2^{64} possible unique values each clock cycle. A 64 x 64 bit planar system could process 64 different 64-bit operations per clock cycle or all bits could be looked at together as potentially representing 2^{4096} possible unique values. This illustrates why the subject of parallel optical processing never really fades away completely. Unless Si-based quantum computing becomes viable there will always be a window for optical processing to do something traditional processors can't. As noted above, quantum computing may actually be on the horizon with the demonstration of a device with the first reprogrammable qubits or quantum bits [10]. The work horse of optical based parallel systems is the spatial light modulator (SLM). This devices allows for control of light in two dimensions (either amplitude, phase, or both). The most common example give is an overhead projector where an LCD is used to perform the modulation which in this example is the projected image. LCD pixels, usually containing three complementary sub-pixels, either block light or allow it through recreating or generating an image. The configuration of these pixels is updated as a function of time. LCDs are by no means the only way to do this. They are appealing because they can translate a digital number into a 2D image. This concept can also be used to perform logical operations. Since light is a wave, Fourier transforms are often employed to do the processing where digital signals are converted to light, processed, then converted back into digital signals or performed directly on light signals. An example of this is a Fourier transform based system that encodes/decodes lower bit-rate tributaries into extremely high 10.8 and 20.6 Tbit s^{-1} data streams [11].

Optical processing systems can be thought of as fitting into two broad categories with respect to hardware: all-optical and hybrid optical-electrical. There are a few instances where all optical operation is a real benefit such as communications where operations to be done on fiber signals [11, 12, 13, 14]. In this field, switching between electrical and optical is a relatively slow operation and is very inefficient. The few times this conversion must be made the better. To transmit information or

very long fiber lengths, optical repeaters are needed to boost signal strength, reform the signals, and retime the signal. These represent the three classifications of optical repeaters. An R repeater is one that only does reamplification, a 2R repeater is one that does reamplification and pulse reshaping, and a 3R repeater does all three including retiming [15]. While hybrid systems are not desirably in the middle of communication chains, they are necessary since most technology people directly interact with is electronic. In the early 2000's a small start-up company named Lenslet announced an optical processor making similar claims to Optalysys; however this endeavor was focused on a computer-like processor as opposed to the large data/server type focus of Optalysys. Although they demonstrated a working prototype in 2003, by 2006 the company had announced it was closing [16]. They produced a single white paper describing a hybrid system called EnLight256 with the promise of a single chip solution that never came [17].
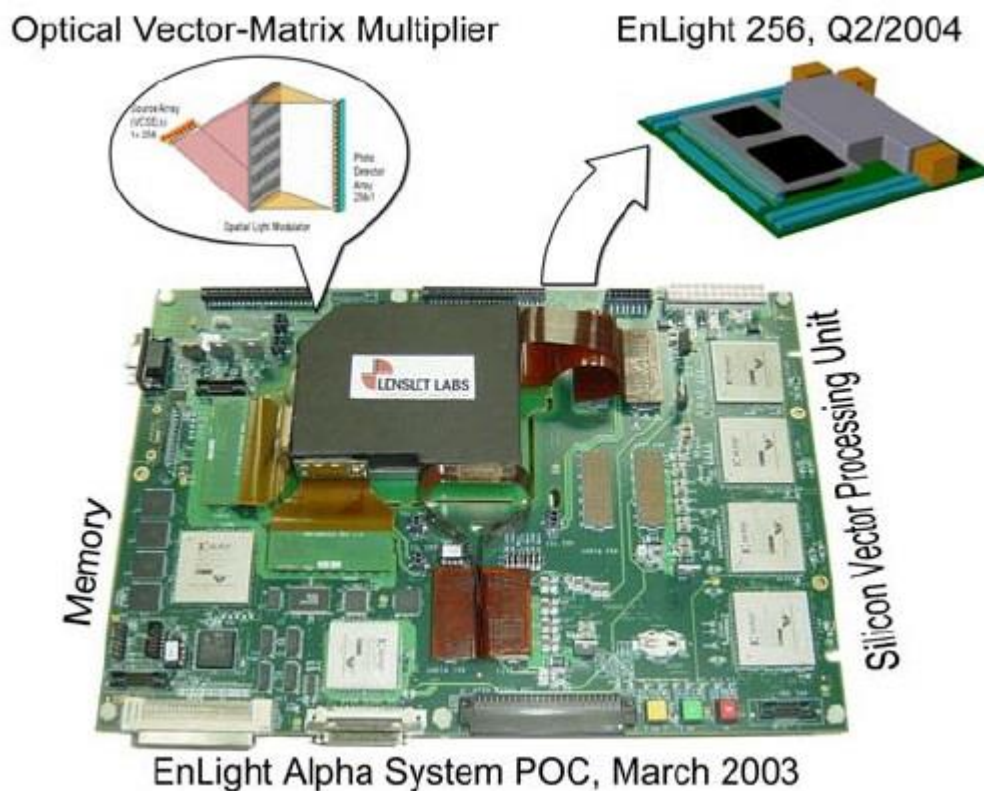
Figure 1. Lenslet EnLight256 single board [17]

Hybrid systems employ some form of electronically controlled manipulation of optical properties. Refractive index manipulation is common, but phase manipulation is also used [1, 2]. Traditionally

these methodologies have struggled to compete with Si-based with transistors on the basis of size. As Si-based transistors have driven from microscale to nanoscale feature sizes with the FINFET (fin field effect transistor) pushing those sizes to the potential physical limits of FET (field effect transistor) technology, moving structures into three dimensions has become an increasingly import subject [18].
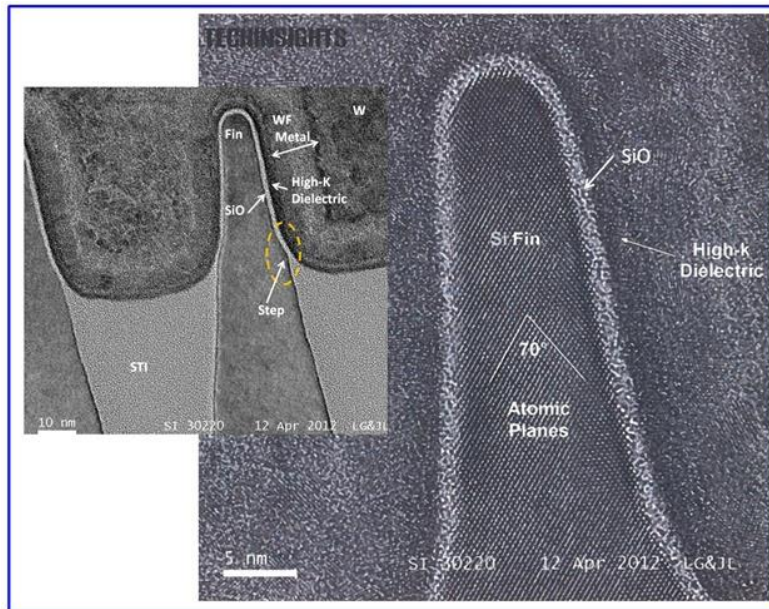
Figure 2. Image of a FINFET [19].

3-Dimmensional Integrated Circuits

Three-dimensional systems were proposed as far back as 1960 with a paper by Jim Early where he discussed issues of temperature and device element density among others [20]. While current papers discuss cost justification and fabrication methods/issues, the subject of temperature is almost always discussed. Thermal budgets are nothing new to IC design. While two-dimensional systems can utilize simple heatsinks effectively, three-dimensional systems run into significant issues that require more advanced techniques such as designing the heat sink into the structure in the form of thermal vias which in turn reduces the maximum theoretical device density [21, 22]. There are significant challenges to three-dimensional structures reaching their promised potential, but there are applications where it just makes sense. One such application is micro electrical mechanical systems (MEMS) where the MEMS devices is fabricated using a Silicon-on-glass process and the electrical system

is most likely fabricated on a traditional CMOS process or something similar. Housing both die in the

same package in a stacked-die configuration makes the most sense [23]. Similar to MEMS, is the idea of

mixing wafers from different processes that are then connected together using through-silicon vias

(TSV) and wafer to wafer bonding [23]. In addition to this, is the desire to utilize multiple active layers

to develop truly three-dimensional wafer-fabricated structures. This would allow for separating

circuitry within the device in advantageous ways like locating memory overtop of a processor core or

placing all NMOS transistors physically below all their PMOS counterparts [24].
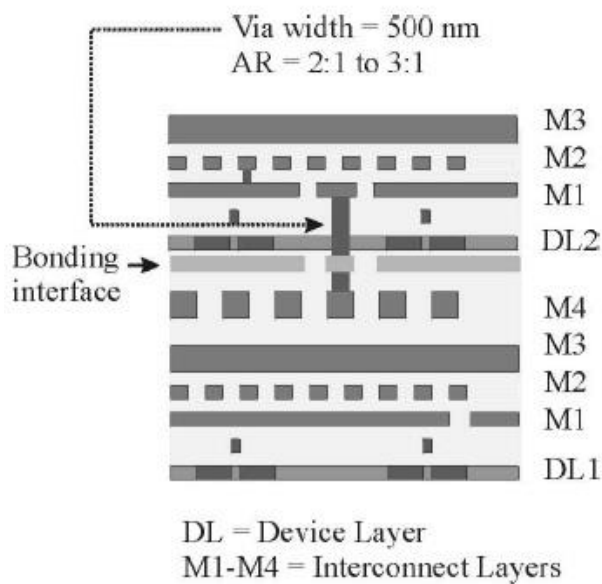
Figure 3. 3D IC Wafer Stack [23]   Figure 4. 3D IC Cross-section TEM Image [24]
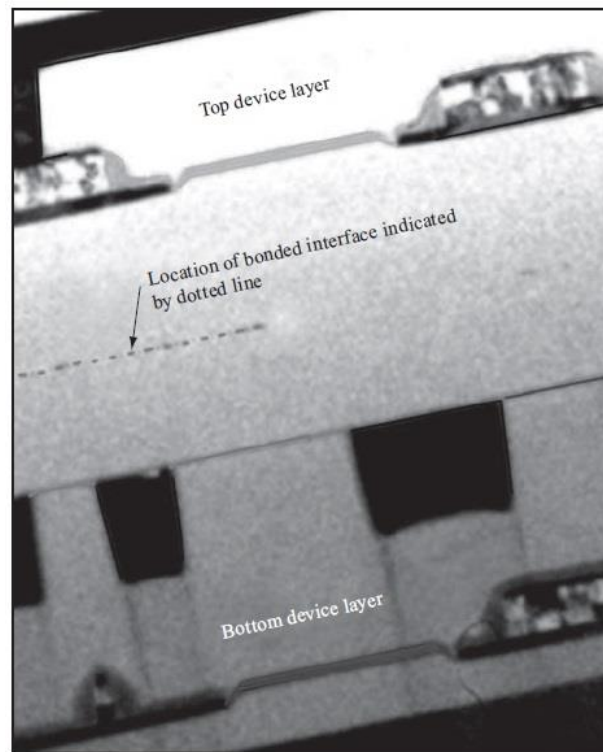
There are two ways circuitry can be expanded in three dimensions: 3D packaging and 3D integrated

circuits. With 3D packaging multiple wafers created using traditional fabrication methods and then

connected using methods like wire bonding or flip chips to connect them. Integrated a MEMS die and a

traditionally processed integrated circuit is an example of this method. There are three methods of

accomplishing this which are described in various ways throughout literature: system in package (SIP),

3D wafer level package (WLP) and package on package (POP). SIP stacks separate dice connecting them with either wire bonding or using bonding points like solder bumps. This is a useful method for building single chip MEMS devices. 3D WLP is very similar to SIC in that TSVs are prepared at the wafer level but the actual connections between dice are made at the package level [25]. POP uses finished die that are connected together in stacks by using an interposer that is integrated into the chips. Connections are made using ball grid array (BGA) connections during PCB processing such that one chip has the solder points available on the top of the device where a different BGA device would get installed [26]. In all of these cases, there is an advantage to testing where individual systems can be tested prior to mating die or wafers together increasing the chances of a finished device that functions properly. Using a fully realized 3D fabrication method complicates testing as a defect on any of the active layers can cause the entire system to fail [27].

The other way of moving into three-dimensions is to make a truly three-dimensional integrated circuit. There are two ways of doing this: 3D stacked integrated circuit (3D SIC) and Monolithic 3D integrated circuits. As previously mentioned, 3D WLP and 3D SIC are somewhat similar since both utilize TSVs, but 3D SIC uses TSVs to directly connect multiple wafers using things like wafer thinning and Cu-Cu contacts. In this scheme, wafers are connected to a dummy wafer for mechanical support, then thinned down as thin as 100µm then connected to another the main wafer stack using wafer alignment techniques [23, 24]. While both wafers are tested prior to being mated there is a risk that a non-functional die location on the wafer stack is mated with a functional die location on the thinned wafer or vice versa thus reducing overall yield [25]. Although this risk exists, being able to mate so many dice at one time does have its advantages over having to mate them one at a time. Monolithic 3D ICs are created using a sort of bottom-up type process [24]. This is where active layers are processed directly onto a wafer using a technique such as Silicon on Insulator (SOI). This methodology solves many of the challenges posed by TSVs like wafer alignment and the fact that Cu-Cu contacts present field risks in large-scale manufacturing environments as the switch from Au to Cu bond wires has demonstrated; however it offers its own challenges such as processing temperature. Doping processes can be upwards of 1000°C, but solid-phase epitaxy can add a doped layer of Si around 600°C. This

process is done by laying down a layer of doping atoms and amorphous Si then heating everything up to crystalize the Si [28]. Creating Monolithic 3D ICs using simpler, more widely established fabrication methods would be advantageous. For example Indium-Tin-Oxide nanoparticles in Niobium Oxide (ITO/NbO$_x$) is a thin-film material that can be deposited using spin-coating then annealed at 400°C [29]. This material however would have to be used with an optical switching scheme rather than an electrical one using traditional transistors. The three pieces needed for such a scheme would be a metal layer, a dielectric layer, and the ITO/NbO$_x$ layer which could all be deposited using industry established methods then etched; the details of which will be discussed later. The tradeoff here is that in order to use simpler fabrication methods, a change from traditional transistors to optical switching would have to happen.

Optical Switching

For reasons previously mentioned, optical switching has generally been tied to telecommunications and data networks as light has always had distinct advantages over wired electrical signals over great distances. Using fiber optic cables as allowed systems to get around Ohm's Law and improve efficiency. Data network usage has drastically increased placing demands on capacity and power that has called for more efficient switches and fewer optical/electrical transitions [30, 31]. This focus on long range transmission and serial data interfaces has affected the constraints placed on problems being researched. In general, the goal is to do all-optical switching of traditional fiber-optic signals. This results in a number of constraints that do not translate well to integrated circuits. One such constraint is the core of a fiber must be larger than the wavelength of the light that travels through it, usually by about five to ten times. This is done to minimize the effects of the evanescent field and diffraction since they remain small compared to the size of the fiber and thus can be neglected. Since integrated circuits have feature sizes from the low micro-scale to the nano-scale that would mean the wavelength of light needed would range from the visible range (1μm/1.24eV) to just into the x-ray range (1nm/1.24keV). While a 1μm wavelength might seem feasible, this would be very old technology with 10μm feature sizes (assuming a 10x relationship between wavelength and feature size). A more common feature size at the present time is 100nm corresponding to wavelengths of 10nm and an

energy of 124eV which is in the ultraviolet range. Even a feature size like this is relatively old

technology with processes now down to 14nm [3]. This is related to another common design constraint

where beam theory is used for the light. This is seen in almost every switching scheme where the

effects of evanescence and diffraction are not dealt with in favor of demonstrating proof of concept

most often by demonstrating the material properties using thin-films. These constraints make perfect

sense when considering their intended use in component-level designs where the entire device is

dedicated to one or two switching operations. These are the designs that are practical for large data

networks. Though any reliable miniaturization or improvement in efficiency or switching speed would

be welcomed by data centers, a large leap in such things are not necessary for data centers to realize

impactful improvements. While component-level processes and physics do not necessarily translate to

wafer-level processes it is well worth considering this large body of work.

An optical switch is a device that controls the flow of photons by a number of effects, with each effect

defining the switch's type. Most of these effects rely on changing the direction of the propagation of a

beam of light, often by changing the refractive index of a material like in bubble switches. MEMS

devices can also directly change the direction of a light beam using micro mirrors. Another approach is

to find some what of blocking or allowing light to pass such as dual polarization like in LCDs or using

destructive interference like in thermo-optic or Mach-Zehnder interferometers [1].

Optical switching by manipulating refractive index is a very common approach. This is because it is

relatively easy to do, is extremely closely related to traditional fiber optic theory, and provides an

acceptable level of accuracy in large data networks where switching speeds are at a far greater

premium than physical device size. This category often ends up being very similar with absorptive and

interference switching as the physical mechanisms end up being shared between the two. The main

difference between the two categories lies in what is done with the beam of light. In refractive index

switching the beam of light's trajectory is changed such that it leaves the device at different location

relative to its original state. This could be thought of as an AB switch or switching between an A and a

B output. Conversely, absorption/interference switching blocks light or allows it to pass. Examples of

refractive index switching are liquid crystal switches, bubble switches, and electro-holographic switches [1]. All of these examples use various physical conditions to change refractive index by applying a voltage to a material. Liquid crystals are perhaps the most familiar as these have been used on very large scales in screens for many years now. In screens, three liquid crystals are placed very close to one another in a grouping commonly called a pixel. Each of the three switches, called sub-pixels, manipulate a specific band of light with each of the three bands making up a complimentary set of colors. The most common set is red, green, and blue. In this configuration, the job of the liquid crystal is to the polarization of the light which is then put through passive polarizer. If the light passing through the sub-pixel is polarized in one orientation, then it is blocked. If it polarized in the opposite orientation, then it passes out of the screen. The three sub-pixels combine to create a signal pixel with a color that can be controlled with voltage and the many pixels combine to create an image. In this case, the liquid crystals are controlling polarization where as in the communications the main goal is to move a beam of light from one place to another. Using a liquid crystal to perform a direction AB switching operation is simply a matter of having two output ports: one port located in line with the expected trajectory of the light traveling through the liquid crystal in the passive state and one port located in line with the expected trajectory of the light traveling through the liquid crystal in the active state. The active state is achieved by applying a voltage to the liquid crystal. In the case of liquid crystal in polymer, a simple structure is employed where as a traditional liquid crystal requires the use of polarizers to achieve the same effect [1].
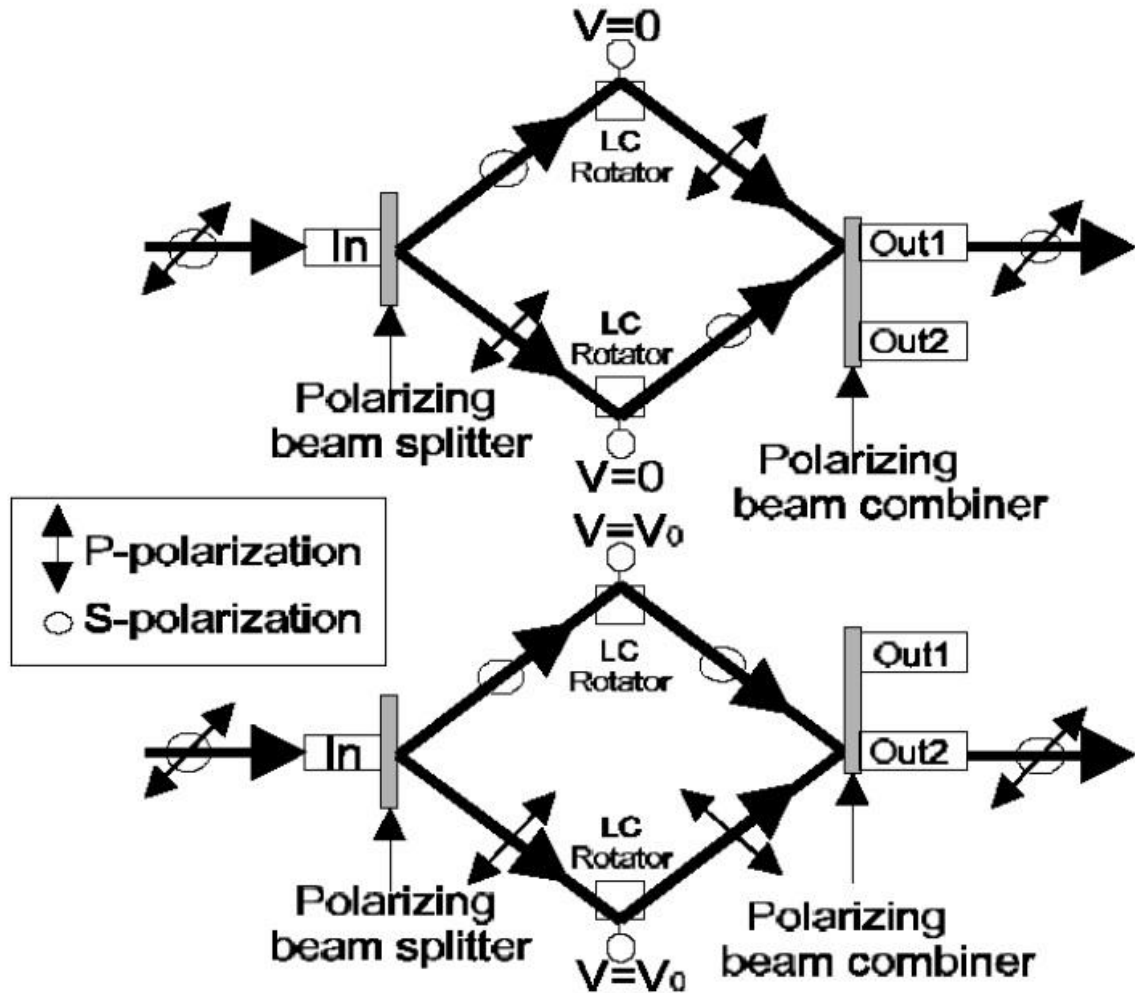
Figure 5. Liquid Crystal Optical Switch Example [1].

An example of a polymer-stabilized liquid crystal switch is a cholesteric liquid crystal positioned

between two Si plates. The unique aspect of cholesteric devices is their potential to continue

functioning when power is removed which has obvious advantages in mobile technology. This specific

example considers infrared wavelengths which of course are of interest in communication networks

[32]. It should be noted that this particular case doesn't make any claims about power usage as its

focus is on the refractive index and polarization. As previously mentioned, liquid crystals generally

have heavy polarization dependencies which combined with passive polarizers makes them a good fit

for displays. What makes this liquid crystal unique is that it is able to effect the refractive index in a

way that is independent of polarization and is also isotropic. This is demonstrated using a Fabry-Perot

interferometer where the polymer-stabilized liquid crystal is positioned between two reflective plates which in this case are Si plates. Experimentation with a gap between the plates of 20μm with respect wavelengths showed modifications to the refractive index changing from 1.58 to 1.49 at 18V with no appreciable change to polarization although voltages lower than 18V did show some continued polarization dependence [32].

MEMS switching consists of using electrostatic control of micro mirrors to redirect light from one port to another. They are generally considered to be highly efficient from an optical loss perspective while also producing very little crosstalk but those strengths are tempered by relatively slow switching speeds and high voltages needed to control the micro mirrors. These voltages often need to be on the order of 10's of volts to nearly 100V to manipulate them, although newer designs have been shown to actuate as low as 0.5V [33, 34].
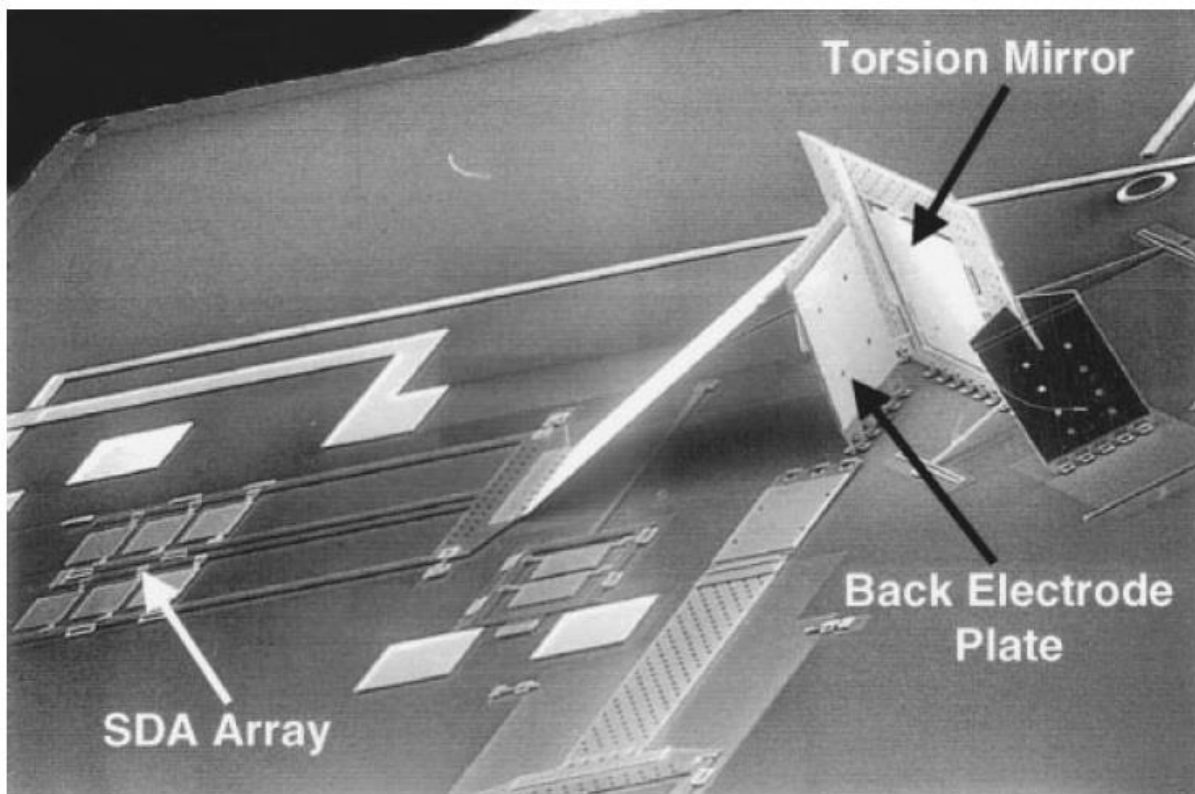
Figure 6. SEM Image of MEMS Torsion Mirror [33].

13

Traditionally, MEMS optical switches relatively slow switching speed best suits them for connections sending large bursts of data over them. Once the switch is configured it is relative cheap from a power perspective thus creating a tradeoff compromising transition speed for lower power. MEMS switches can be used in combination with switches based on other technology which transition faster to create systems that can leverage the strengths of MEMS switching while also using the versatility of the other technologies to meet both the bus load and plasticity demands of modern networks [30]. The micro mirror can be applied in a number of ways. Torsion mirrors pivot a micro mirror in one or two dimensions where the light comes in at some angle from above the die surface and is angled to another location in the device. Changing the angle of the mirror thus redirects the beam a light to a different port. Another approach is the direct light to a port using a fixed mirror then having another mirror that can be moved into the path of the light directing it to a different port [35]. Since most designs rely on beam theory, smaller scale structures are problematic. Even designs that use diffraction to their advantage are still technically using beam theory for much of the system such as is the case with a switch combining a micro mirror and a Fourier lens [36].

Aside from redirecting light, it can be blocked. This can be accomplished in two ways: absorption and destructive interference. Absorption is kind of the brute force method to switching. Instead of worrying about exactly where the beam is headed or what other effects may be present, it's all sent through or none is. This is analogous to digital logic. It differs from digital logic most critically in the area of power. MOSFETs work by using fields to allow charge flow or prevent it. The main power draw in these devices is the actually switching which consists of the charging and discharging of the gate capacitors. In absorptive switching the device must absorb and dissipate all the energy entering it when in the blocking state which means heat. Heat management is a very important issue when discussing any IC especially 3D ICs. Absorption and destructive interference is an area where research has focused on in recent years. Nanowires and nanoscale objects are of specific interest as researchers keep pushing dimensions smaller with MOSFET gates in the 20nm range. In nano-structures, light interacts with materials by a process called plasmonics. This is concept that helps describe how things like metals interact with light since the large number of mobile electrons in metals makes them behave

similarly to plasmas in electromagnetic fields. Plasmonics does a good job describing how light with a wavelength greater than the dimensions of a nano-structure interacts with that structure and will be discussed in greater detail in a later section about material properties. An example of an optical switching using plasmonics is a low voltage broad band hybrid plasmonic-vanadium dioxide switch [37].
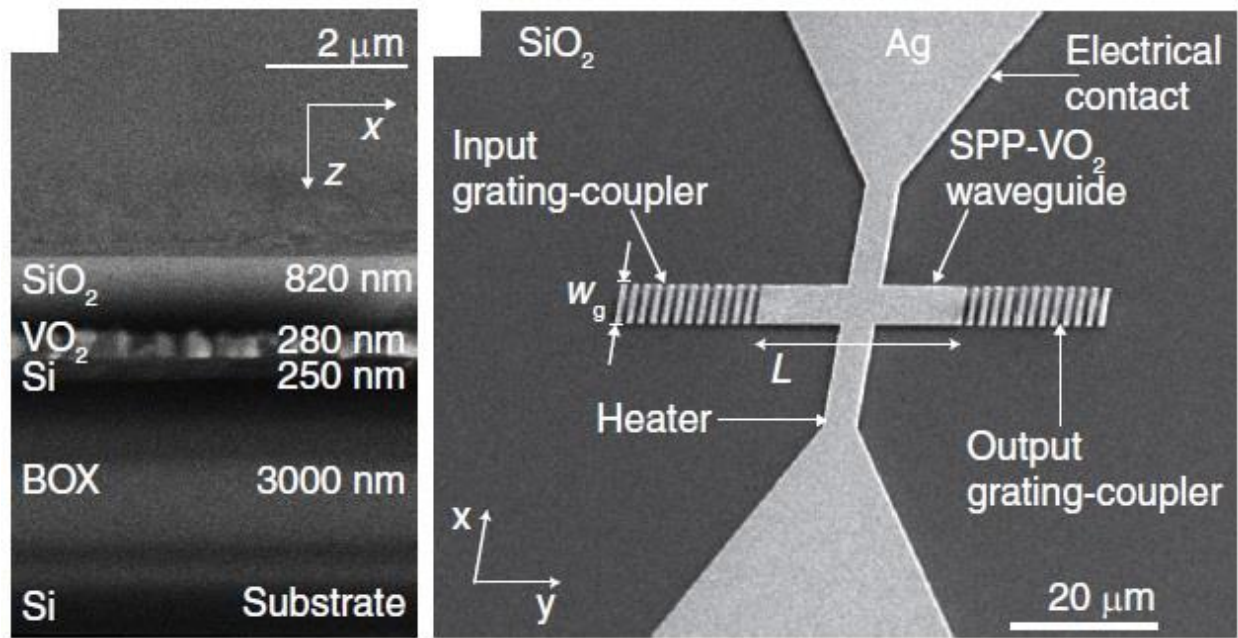
Figure 7. SEM Images of a VO$_2$ Plasmonic Heater Switch [37].

This is a sub-wavelength plasmonic switch relying on VO$_2$'s phase changing properties. The switch uses grating-couplers made from the VO$_2$ light guide overtop of an ohmic heater built out of silver to create the switch. The grating-couplers exist to get the light into and out of the switch with the active region of the switch being the VO$_2$ light guide. A voltage is applied to the silver electrodes produces localized heat under the VO$_2$ light guide causing the phase shift resulting in an increase in extinction ratio: direct absorption in VO$_2$. It serves as an important proof of concept with the dimensions of the switch being roughly 80μm by 60μm. It should be noted that most of this area is taken up by structures necessary to properly test the concept of the device like the electrodes which are significantly larger then would necessary in a fully integrated device. The width of the VO$_2$ light guide is 8μm, the thickness is 280nm, and it has a length varying from 5μm to 15μm and the wavelength of the light being 1.55μm. While this is not small enough for dense integrated circuits, it does demonstrate the principles well. It should

15

also be noted that wave-guide dimensions smaller than 10x the wavelength of the light traveling through them can be considered sub-wavelength since below this point all the issues associated with sub-wavelength light guides begin to come into play. This VO2 switch has a light guide only 5x larger in width and a little over 5x smaller in thickness than the light's wavelength. Due to silver being used for the heating element a low activation voltage of 0.4V was reported [37]. Based on the dimensions given in the paper, an activation voltage of 0.4V and an assumed localized temperature around 75C corresponds to something on the order of 40μW.

A type of destructive interference switching based on the self-collimation effect in photonic crystals has been proposed on a theoretical basis since at least the early 2000's [38, 39]. The self-collimation effect is that beams of light propagating through perfect photonic crystals effectively ignore many of the unwanted small feature size effects that cause the beam to disperse.
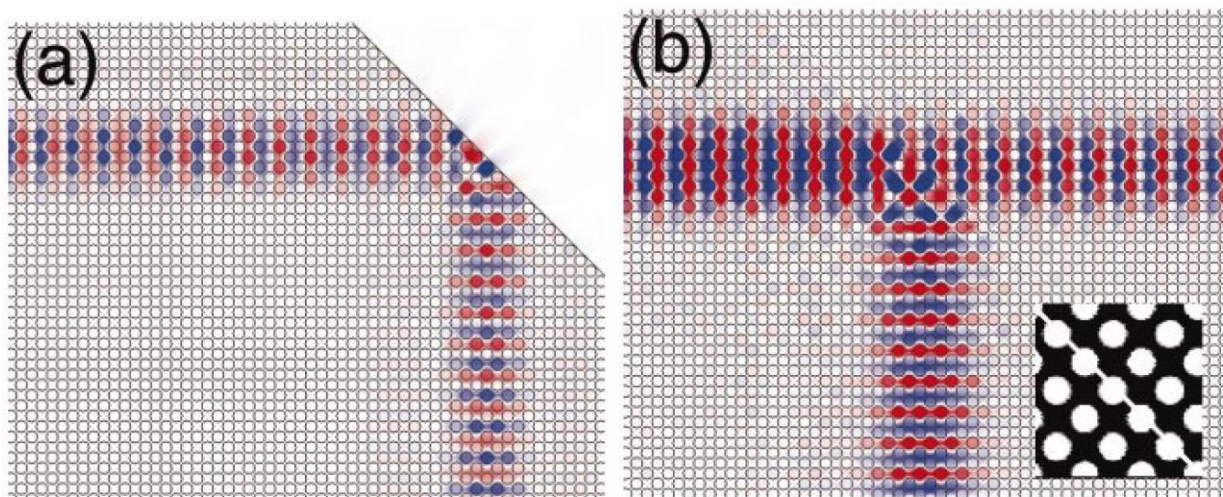
Figure 8. Magnetic field distribution of a self-collimated beam propagating through bend (a) and splitter (b) [38]

Feature sizes claimed in these papers are on the order of lattice constants of the photonic crystals. For one such example, the photonic crystal is silicon rods in air [39]. This design consists of a square layer of silicon with air holes arranged in a repeating lattice structure. Along one diagonal of the structure there is a single line of air holes with a smaller radius than the rest of the structure. This

16

creates a 3dB splitter where a beam of light entering on side of the structure is outputted both in the transmitted direction but also one perpendicular to the original trajectory in the reflected direction. The transmitted beam sees no phase shift but the beam that is reflected at a 90° angle and is phase shifted 90°. The inputs are perpendicular to one another as are the outputs such that there is always a transmitted direction and a perpendicular direction for each input. One input's transmitted direction is the same as the other input's perpendicular reflected direction. If a beam of light of the same wavelength enters both inputs with one of the beams phase shifted 180° then one output sees constructive interference and the other output sees destructive interference. Exactly which output sees what, is a function of the incoming beam's phase shift. The proposed design is a $12\sqrt{2}a$ by $12\sqrt{2}a$ square of silicon with air having a radius to lattice constant of 0.35 [39].
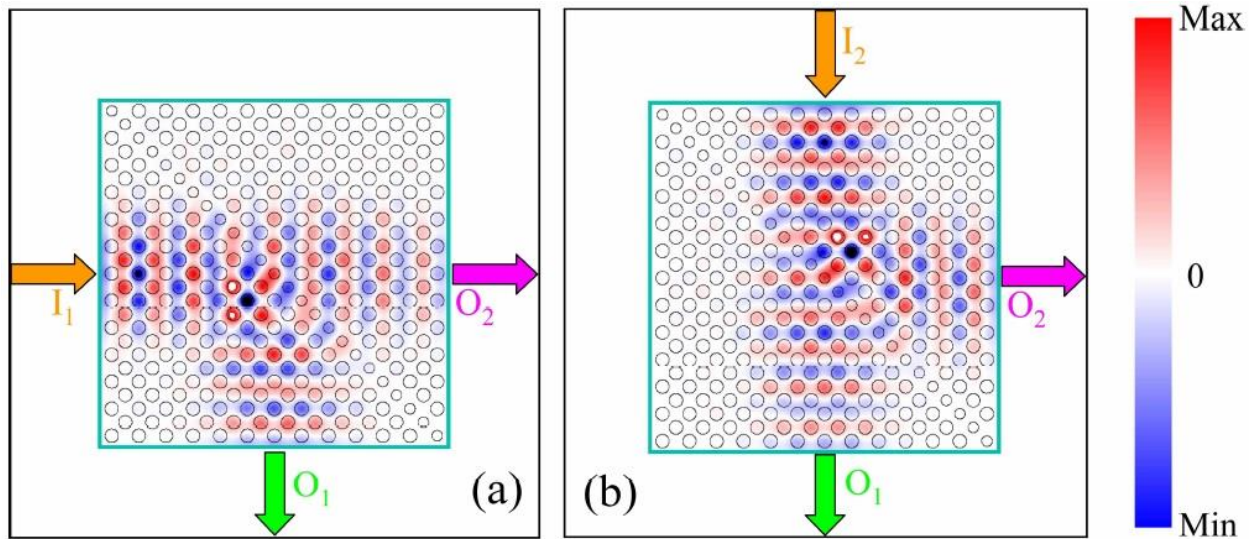
Figure 9. Self-collimated AB switch [39].

The proposed design and subsequent simulations do not consider any finished dimensions but rather keep things in normalized terms. The dimensions of photonic crystals are generally referenced to the desired wavelength. For example, a common wavelength in fiber optic networks is 1550nm making the lattice constant about 525.5nm [40]. This would make the proposed structure about 8,918nm by 8,918nm which is quite large when compared against current FET technologies. Extrapolating this relationship out to the limits of visible light results in structures with side lengths of 4,027nm (λ = 700nm, red) and 2,301nm (λ = 400nm, blue). Even into the near ultraviolet range the side lengths only

17

get down to 575.3nm (λ = 100nm, ultraviolet) which is a full order of magnitude larger than current FET process feature sizes. Despite this possible short coming for integrated circuits, this design provides an interesting possible solid state switching solution for communication networks which is likely its intended application.

The switches discussed thus far focus on devices that switch an optical beam on or off. There is also the need to eventually convert that light back into electricity if used in an integrated circuit. While this is a deep field of study by itself and falls somewhat out of the scope of this paper, it is worth mentioning a couple of them. ZnO nanowires were shown to have an optically induced, reversible resistance change making them a potential option for photon/electron conversion [41]. The nanowires were analyzed with diameters ranging from 50nm to 300nm. They were exposed to light with wavelengths below 380nm and were found to have resistance changes of 4 to 6 orders of magnitude with a high level of sensitivity. It was also confirmed the ZnO nanowires were not responsive to wavelengths above 370nm which is a material dependent cut-off for the effect [41]. InP nanowires were shown to exhibit anisotropy with respect to polarization [42]. These were analyzed in air such that the refractive index difference between the air and the material was larger than it would be in a normal semiconducting environment. In addition to this sensitivity to orientation, the nanowires were observed to change their conductance by two to three orders of magnitude [42]. These findings suggest the materials could be an interesting option for detection applications since any switching operations would require changing the orientation of a beam of light or the nanowires themselves. Positioned correctly with respect to the phase of light guide, nanowires can also be used to absorb light. An example of gold nanowires placed on top of SOI waveguides shows how the phase of the light effective can control whether it is absorbed in the nanowires or not [43]. Unlike some of the other nanowire examples given, this is a direct plasmonic effect. The gold nanowires where simulated with the width and thickness held constant at 40nm and 25nm respectively. The antennas were laid on top of and perpendicular to the waveguide such that varying the length of nanowire effectively changed the cross-sectional area the nanowire could cover. The simulations showed that the optimal condition was three equal sections of gold nanowire 105nm long, spaced 40nm apart for a 400nm wide and 200nm

thick Si waveguide and a wavelength of 1550nm. It is important to note that the effectiveness of the nanowires is wavelength dependent. The interactions between nanowires and light can be thought in a similar fashion to electromagnetic waves interacting with antennas whose lengths are shorter than the fundamental wavelength of the incoming wave. Two waves are fed into the waveguide with the same frequency and phase matching such that a standing wave is produced with the nanowires positioned at one of the power minimums thus minimal absorption by the nano wires takes place. By shifting the phase of this standing wave, the location of the power maximum shifts to the same location as the nanowires allowing for maximum absorption. An example of combining this basic structure into a switch is given using an evanescent X-coupler. This is a device that routes two waveguides very close together such that the evanescent field from one guide bleeds into the adjacent waveguide transferring some power between the two. Each light guide has three rows of three nanowires positioned in same place with respect to its adjacent lightguide's nanowires. Waves enter both inputs with the transmission or absorption depending on the phase of the resulting standing wave. In the event of absorption, the standing wave's power maximum is shifted to the location of the nanowires providing maximum absorption and minimum power transferred through to the two outputs. Conversely when the power minimum is shifted to the location of the nanowires, minimum absorption occurs allowing for the maximum power to be transferred to the two outputs. This effectively creates a phase dependent switch which functions similarly to a Mach-Zehnder interferometer. The key difference between the two is a Mach-Zehnder interferometer functions more like an AB switch rather than an on/off switch [43]. This example is still large by comparison with the full structure being at least in the low micrometer range. It is interesting from the perspective of relying on more readily available manufacturing processes like SOI and metal deposition. Reading the various properties of different nanowires illustrates the material dependencies there are in the subject of lightguides and optical switching.
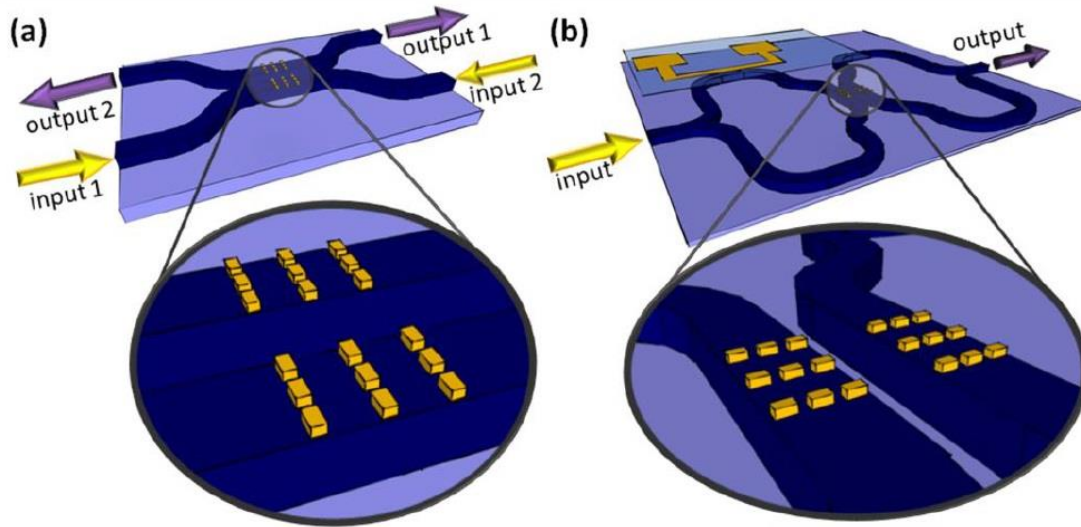
Figure 10. Optical switch (a) and modulator (b) using gold nanowires on top of an SOI evanescent X-coupler [43].

Optical Properties of Materials

The optical properties of materials essentially is a discussion of how electromagnetic radiation interacts with materials. Generally when talking about optics, the discussion is limited to the wavelengths around the spectrum that is visible to the human eye. With this distinction in mind, the properties important to consider are absorbance, birefringence, reflectance, refractive index, and transmittance. Absorbance, reflectance, and transmittance effective describe what happens to the energy at a material interface and in the material. Reflectance describes how much energy is reflected back from the material interface, and transmittance describes how much energy moves through the material interface. Absorbance describes how much energy is lost to the material as the radiation moves through it usually in the form of photons transferring energy to electrons. Refractive index is the relationship between the radiation's phase velocity in the material and in a vacuum. The classical consideration of this property is to describe how a light ray is bent moving through a material interface. Birefringence is a property where the refractive index of a material is a function of polarization. Often a polarization independent switch is desired which allows for a more generic switch that can easily be placed into any situation and still function, but this is situationally dependent. For switching applications material properties that are not static are desired. An example

20

of a liquid crystal that has a polarization-independent change in refractive index was given in the prior section [32]. Other switches rely on changing the absorbance of a material. For effective integration into electrical systems, this changed would need to be controlled electrically whether directly like in the case of electrochromic materials or indirectly like with VO_2.

Plasmonics is an effective way of describing how light interacts with electrons in materials like metal. In metal, there are a large number of free electrons such that can interact with an electric field. This is similar to a plasma where all the electrons of a material have been given enough energy to be free electrons. In the presence of an electric field, these free electrons are attracted or repelled by the field and thus move. When this electric field is alternating like is the case with light, these electrons are alternately attracted then repelled as the polarity of the field changes. This interaction absorbs some of the energy from the light; however this attenuation is wavelength dependent. Eventually, the electrons reach a maximum speed as they move back and forth and increasing the frequency no longer has any effect. This higher frequency light can pass through the plasma with no effect due to the electron attraction/repulsion interaction. Since in metal there is a similarly large number of free electrons, there is a very similar interaction between light and the electrons. Like in a plasma, at some point the electrons reach a maximum speed and can no longer interact with higher frequency light. The frequency at which this happens is proportional to the color seen reflected back from a metal. This is only the most obvious and observable effect described by plasmonics. What makes plasmonics of interest in optics is the electron attraction/repulsion effect holds true for objects much smaller than the wavelength of the light: for example how infrared light ($\lambda \approx 1550 \mu m$) interacts with a gold nanoparticle ($d \approx 20nm$). Considering the simplest case where a spherical particle is exposed to light, the electromagnetic field pushes and pulls on the electron cloud in the material due to the Coulomb force; the motion of which is called a dipole plasmon resonance of the particle [44].

21
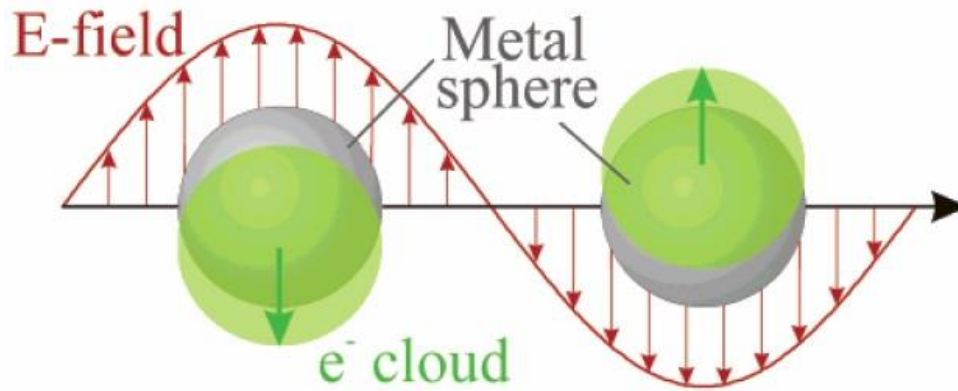
Figure 11. Schematic for plasmon oscillation for a sphere [44].

When half the electron cloud moves parallel to the electromagnetic field and half moves perpendicular, the plasmon excitation is called a quadrupole mode. Relating higher mode plasmon resonance can be very complicated like when it relates to d-orbital electrons, but this can be related to the dielectric constant of the material. In the case where the particle is much smaller than the wavelength of the light, the electromagnetic field can be considered constant. This is known as quasi-static approximation. For more complex particle shapes, numerical methods are needed to describe their plasmon resonance. The Modified Long Wavelength Approximation for spheroids is based on the quasi-static approximation which can effectively show the red shifting as the spheroid becomes oblate. Beyond that, an effective way to describe plasmon resonance is the Discrete Dipole Approximation (DDA) which looks at structures as made up of individual discrete dipoles which have solutions to Maxwell's equations, and solve for the final structure numerically. It should be noted that other numerical methods exist such as multiple mutipole method and the finite difference time domain method each with their own advantages and disadvantages [44]. Looking at complex structures as composites of simpler geometries has been used to look at things like triangles, cubes, cylinders, spheroids and concentric spherical shells [44, 45, 46].
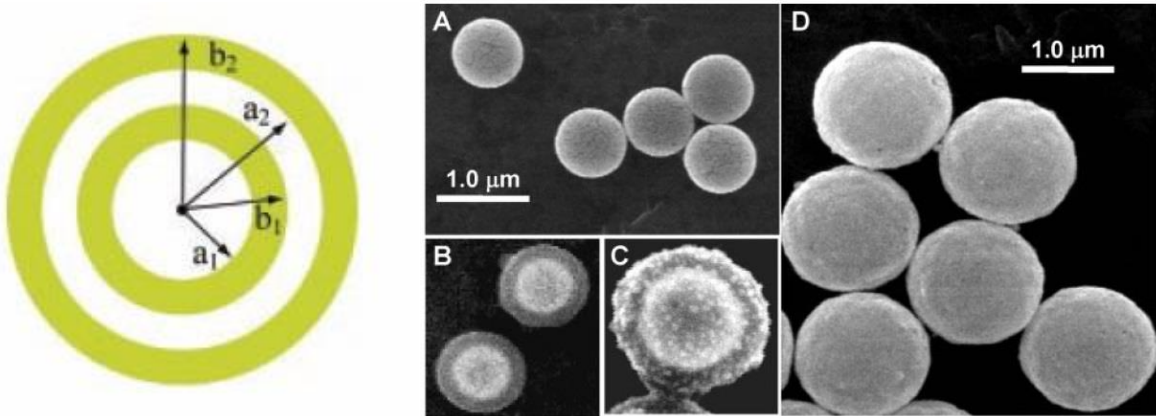
Figure 12. Au-silica concentric shell particle and SEM images showing the silica particle (A), the Au coating on the silica (B), the second layer of silica (C), and the second Au coating on the finished concentric shell particle (D) [45].

In addition to the shape of a particle having a major influence, the proximity of a particle to other particles also has an impact. The closer two particles get to one another, the more they act like a single larger particle. In the case of two spherical particles, they will act increasingly as a single spheroidal particle red shifting if aligned in the parallel direction and blue shifting if aligned in the perpendicular direction [47]. In the parallel direction, the two spherical dipoles reinforce one another since the positive end of one is near the negative end of the other resulting in an additional attraction force in addition to the applied electromagnetic field. In the perpendicular case, the ends of the dipoles end up near their like-charges resulting in a force that effectively works against the applied field [47].
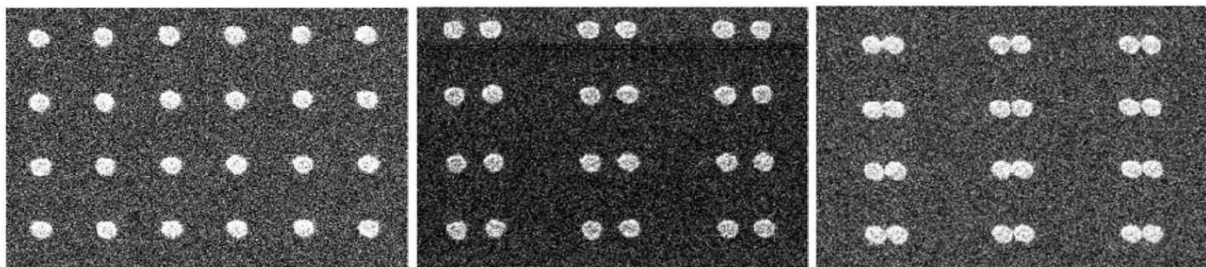
Figure 13. SEM images of Au nanoparticle pairs (diameter 150nm) spaced center to center distances of 450nm, 300nm and 150nm (left to right) [47].

Theoretical study of the plasmon resonance behavior of nanoparticles shows a very strong dependence on size and shape which has interesting implications, but it also yield very practical problems for experimentation. If one wants to gather measurements on spherical nanoparticles, how closely the particles are to perfect spheres will have a major impact on the results. Often making large quantities of particles results in a relatively large variation of sizes and shapes which both theoretical work and experimentation have shown to significantly change the results [48]. While complex shapes can be challenging, they also have been shown to have interesting results. Such is the case with a spherical concentric shell made from $BaTiO_3$-Au-SiO_2. The core is made from $BaTiO_3$ with a very thin shell of Au which is then surrounded in SiO_2. This structure was shown to produce a difference-frequency generation effect which is a stepping stone in developing an optical parametric amplifier [49].
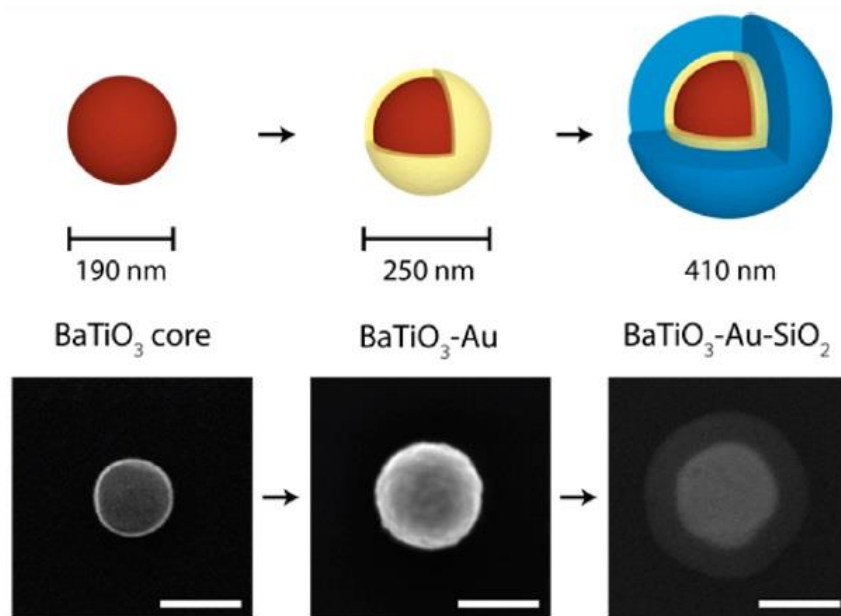
Figure 14. Schematic and SEM images of a BaTiO3-Au-SiO2 concentric shell nanoparticle [49].

The difference-frequency generator discussed here effectively combines an input signal field with a very strong pump field producing an amplified field with the wavelength that is the difference between the signal and pump fields. Another interesting practical application is using surface plasmons to probe semiconductors in a touchless manner [50]. The surface plasmon effect has primarily been studied in metals, but technically anything with an excess of charge carriers has this effect contributing to its

behavior in the presence of an electromagnetic field. Charge carriers in metals are on the order of $10^{23} cm^{-1}$ while Si-based semiconductors can be on the order of 10^{16} to $10^{21} cm^{-1}$ depending on doping. Since current doping processes are inaccurate when compared to the needs of controlling nanoparticle properties, significant challenges exist; however being able to probe using surface plasmons provides a new way to determine localized properties of materials and these effects become more dominant as structures get smaller.

A material that garners attention due to its relatively unique properties is Vanadium Dioxide. This material is able to undergo a phase transition at relatively low temperatures. This phase transition happens between 66°C and 68°C. Specific to the material's electrical properties, there is a semiconducting to metal transition where properties like resistance and opacity in the infrared range can change by up to four orders of magnitude. Below the transition temperature, VO_2 is transparent to infrared wavelengths and above in the metallic state becoming reflective [51]. It should be noted that sources alternate between calling the room temperature phase of VO_2 between "insulating" and "semiconducting". The physical effect being described is a sort of low conductance. Likely papers discussing the material properties in terms of resistance are more likely to call the low conductance state "insulating" whereas papers looking at other properties might be more likely call it semi-conducting. "Semiconducting" is probably a more accurate description since the effect is reversible and doesn't cause any obvious physical damage which makes for a good distinction between "insulating" and "semiconducting". While the semiconducting and metallic phase transition is a temperature based effect, it has been shown be possible to locally affect material properties in a way that is analogous to Si-based transistors or diodes with a current conducting channel whose width varies proportional to the current flowing through it. This demonstration places two Ti/Au electrodes on a layer of VO_2 with a 15μm gap between them [52]. The increase in current flowing through the channel has a self-heating effect where more current means more ohmic-heating and thus more VO_2 transitioning into the metallic phase with the maximum width of the channel being the width of the electrodes at the gap.
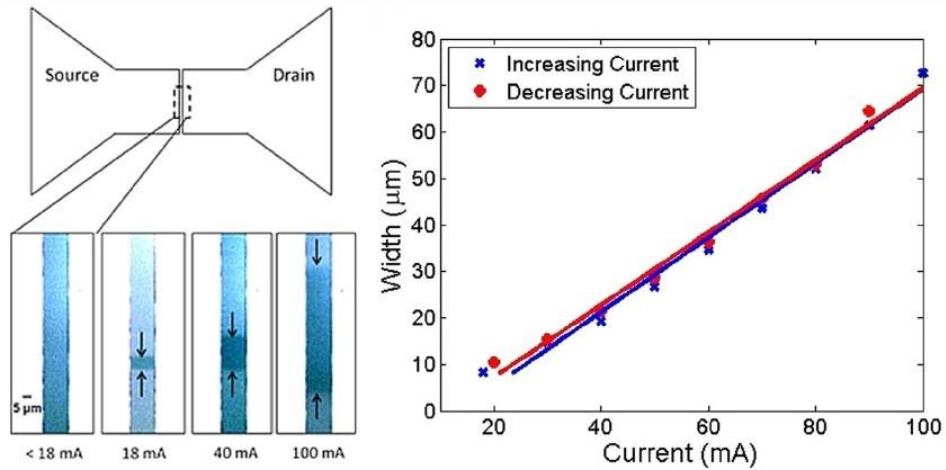
Figure 15. VO$_2$ transistor showing self-heating that is proportional to channel width in the VO$_2$ [52].

In the metallic phase, the transmittance decreases. Comparing VO$_2$ thin films to VO$_2$ nanoparticles shows a significant difference in this property. The thin film shows superior transmittance changes but this comes at cost. The overall transmittance is lower and the reflectance is higher in the semiconducting state [51]. Additionally the greatest transmittance difference between the semiconducting and metallic states happens at long wavelengths, 2000µm to 2500µm. The nanoparticles show a region near 1000µm to 1500µm that shows a comparable transmittance difference. Also, the overall reflectance of the nanoparticles is quite low. Smaller wavelengths mean smaller feature sizes and less reflectance means less light is reflected at interfaces which helps with managing noise when devices are jammed very close together.

26
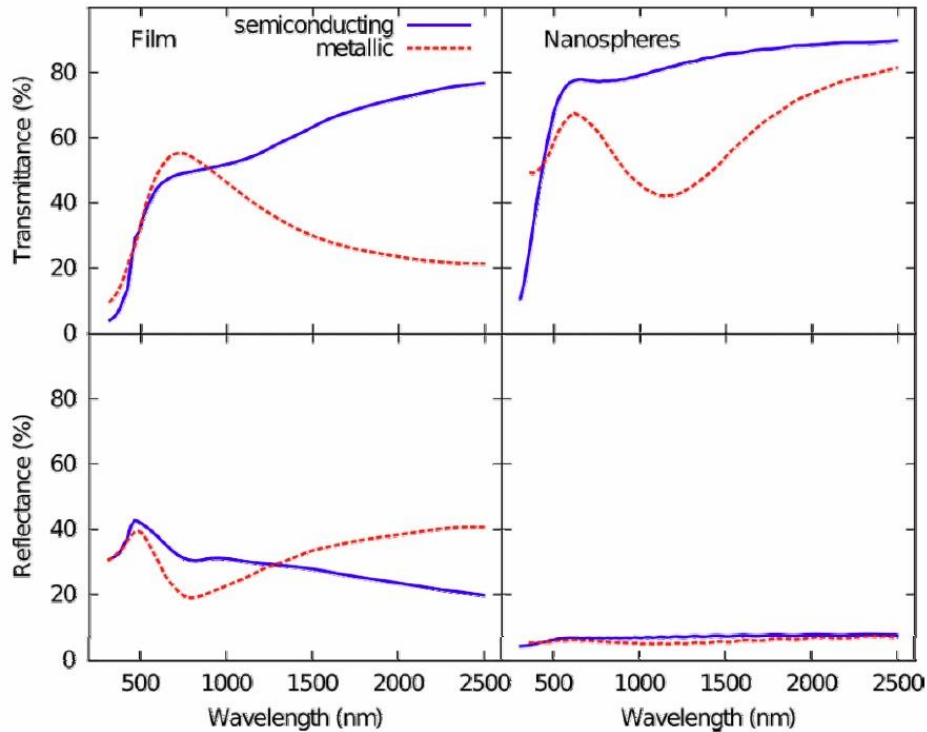
Figure 16. Transmittance and reflectance of VO$_2$ film and nanoparticles above and below the transition temperature [51].

Experimentation by adding gold nanoparticles to VO$_2$ showed a change in resistivity of four orders of magnitude and a small decrease in transition temperature [53]. The sample was prepared by alternating a number of laser pulses between high purity Vanadium and Au targets in the presence of a Sapphire substrate until the total thickness of the VO$_2$/Au was 200nm. All the other parameters where in line with pure VO$_2$ but the transitions temperature was about 3.3K less when heating up and about 3.5K less while cooling down. This difference was attributed to the presence of Au nanoparticles acting as electron sources. This idea was taken to the nanoscale where Au nanoparticle coated VO$_2$ nanoparticles where shown to have ultrafast switching properties. Picosecond laser pulses where used to generate hot electrons that are injected across the Au/VO$_2$ interface inducing sub-picosecond phase transitions of the VO$_2$ [54]. Samples of nanoscale VO$_2$ coated with Au nanomesh were hit with 60ps laser pulses with the samples near the 68C transition point. This produced a nearly step-like response

27

as measured by monitoring the response at 3100nm which was chosen to maximize the difference between the metallic and semiconductor states.
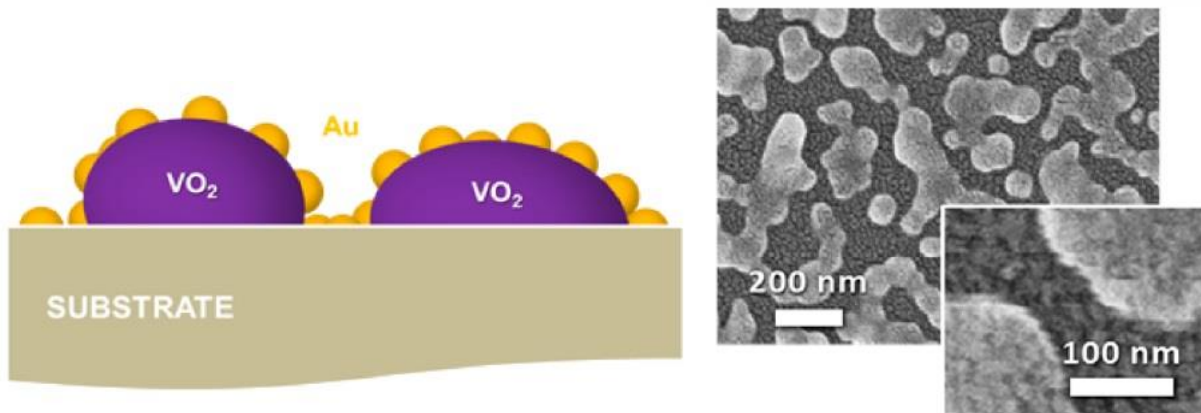
Figure 17. Au-coated VO$_2$ nanoparticles [54].

Graphene is a form of carbon that is effectively two-dimensional. It is a single atom thick lattice of six carbon atoms linked in a hexagonal configuration. Graphene has many interesting properties like its high strength to weight ratio, electron mobility, and thermal conductivity. Graphene by itself is a more like a metal than a semiconductor with a 0 eV band gap. Introducing oxygen produces a non-zero bandgap. It has been demonstrated that graphene oxide can have its bandgap, and thus its optical properties, tuned by using IR radiation, varying the exposure time and power to shift the absorption and photoluminescence [55]. In addition to graphene oxide, Graphene ribbons have shown optical properties like photoluminescence as well. These properties are highly dependent on the size and shape of the graphene [56]. Graphene has also shown charge carrier mobility dependence on substrate material as well. SiO$_2$ is often used, but the roughness which can cause scattering or charge traps. Hexagonal boron nitride has been shown to improve mobility by an order of magnitude. Atomically flat substrates produce a very low mobility while layered dichalcogenides, semiconductors made from transitional metals and elements from the oxygen family, appear to have the potential for good substrate material [57]. This brings up the potential need for substrate material that is less common and most likely more expensive than Si. A surface plasmon polariton (coupled photon and electron) modulator has been proposed using graphene on a lithium niobate substrate. Depending on the

polarization of the lithium niobate, a surface plasmon polariton in the graphene will be absorbed or pass through [58]. When the lithium niobate is down polarized, the surface plasmon polariton energy is highly consentrated near the surface of the graphene and when the lithium niobate is depolarized, the energy flows into the graphene where it is absorbed. Control over the polarization of the lithium niobate results in the electrostatic doping of the graphene with the example given in literature being p-doped graphene in the down polarized state [58].
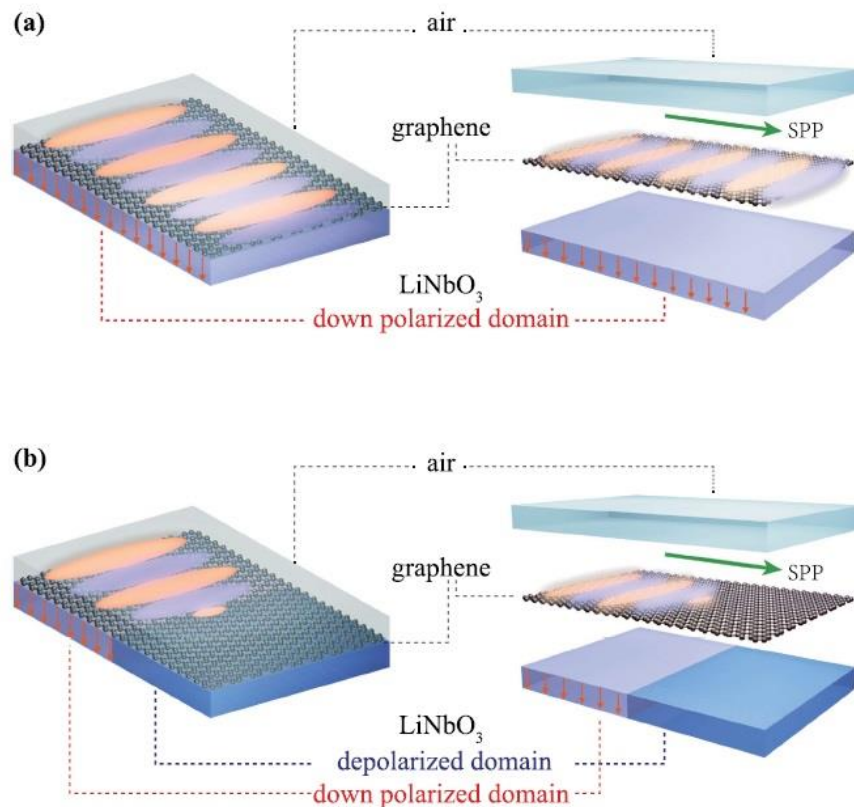
Figure 18. Surface polariton plasmon propagating at the surface of the graphene in the region of LiNbO₃ that is down polarized (a) and being absorbed in the depolarized region (b) [58].

Combining graphene with other materials like cadmium sulfide (CdS) has been shown experimentally to enhance the nonlinear optical properties of organic glass like polymethyl methacylate [59]. Testing compared samples with varying degrees of graphene/CdS with respect to transmittance and absorption. Interestingly, the results showed that simply increasing the graphen/CdS didn't necessarily increase the absorbance of the material. Various concentrations and combinations were tested such as the glass by

itself, graphene in glass, CdS in glass, and the various concentrations of graphene/CdS. There was one specific concentration of graphene/CdS that appeared to outperform the others (7.8mg dispersed in the glass). These results are attributed to three things: the structure of graphene causes the material to have a large number of delocalized electrons which enhance nonlinear optical effects, the CdS nanoparticles on the graphene allow for a large number of light active sites, and the charge transfer between the graphene and CdS suppresses charge recombination [59].

Indium tin oxide (ITO) has been used in displays for many years because of its ability to conduct current while allowing light to pass. This is used as a thin film on glass that functions to connect things like LCD pixels with their driver chip pins. ITO is an n-type degenerate semiconductor with an optical bandgap of around 3.75eV. This bandgap makes it mostly transparent in the visible light range and opaque in the infrared and near infrared range [60, 61]. The conductivity of the ITO comes from the high carrier concentrations which result from oxygen vacancies and tin dopants [61]. The form that ITO comes in can have an impact on its properties. Experimentation with RF sputtering on quartz substrates show significant metal grain structure variation with respect to substrate temperature. This ranges from amorphous ITO to polycrystalline which was verified both in SEM imaging and X-ray diffraction measurements. In addition to grain structure changes, the temperature also resulted in an increase in the carrier concentration that tracked increasing substrate temperature and a shifting and changing of the refractive index curve [61].
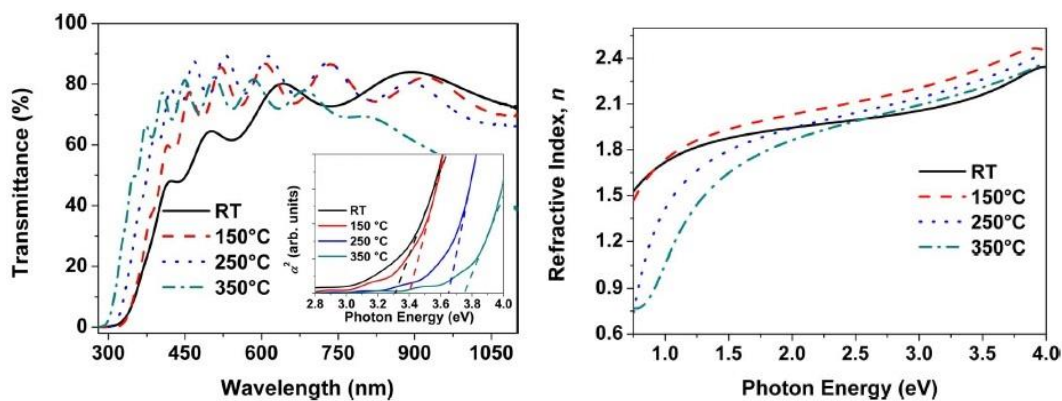
Figure 19. Transmittance and refractive index of ITO that is prepared with RF sputtering on substrates of varying temperature [61].

Thin films made from ITO nanoparticles experience similar results during annealing. Experimentation varying annealing temperature and time showed similar results to the RF sputtering on the heated substrates. This testing showed a similar change in conductance near the 250C mark, but then went on to show the conductance begins increasing again. In this study, the decrease in conductance near the 250C mark is attributed to a decrease in carrier concentration due to oxygen diffusion into the ITO [62]. It attributes the increase in conductance at very high annealing temperatures (up to 1000C) to sintering of the ITO nanoparticles which was shown visually through SEM imaging. Similar results were reported by an earlier study which showed the same sintering at 800C along with the same changes in conductance and transmittance [63]. It was also shown that annealing time also can result in a decrease of conductance by testing various times while annealing at 550C. This was carried out in ever increasing time increments until eventually annealing for 4080 minutes, showing the conductance effectively maxes out at the same value as the initial peak near the 25 minute mark. In addition to this, both annealing temperature and time was shown to also increase the range of wavelengths with good transmittance. This was attributed to the decrease in carrier concentration which was reported to happen faster than the decrease in measured conductance [62]. ITO nanoparticles have also been shown to have dependencies on Sn doping levels. This produces a shift in the absorption that is associated with charge carrier concentrations which is consistent with ITO bulk and thin-film results [64]. As dopant levels increased, it was noted that the doping became less uniform and began showing significant sample to sample variation. This shifting was explained as a Sn building up on the outsides of the nanoparticles resulting in a structure that is closer to a concentric spherical shell described in several papers on plasmonics [45, 46]. The resulting of this Sn build-up was a semiconductor-like behavior with the center of the ITO particle having a different Sn content than the outside. Conductivity experiments supported the Drude model descriptions of particles having large potential barrier from particle to particle consistent a depletion region near the surfaces of the particles [64].
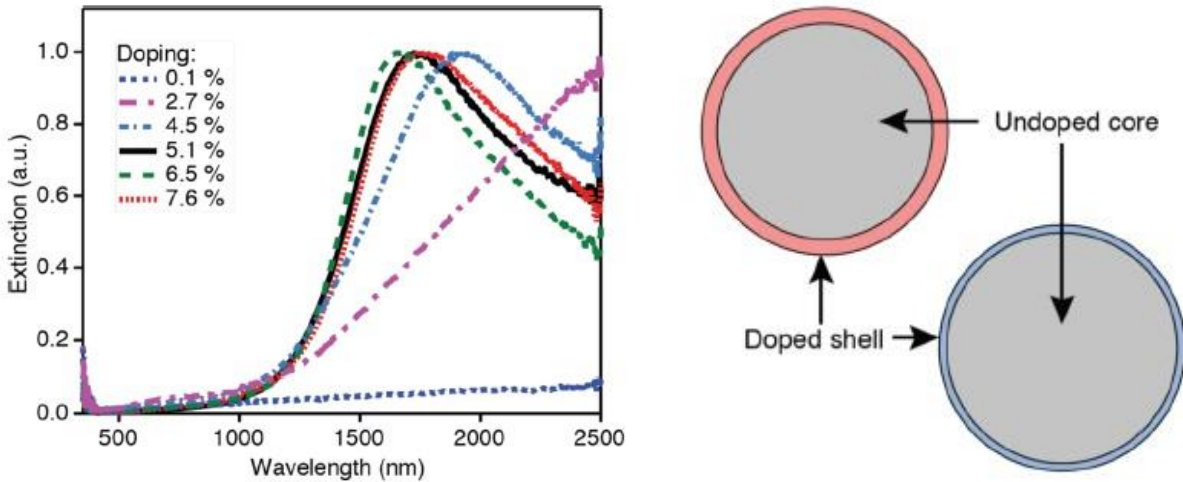
Figure 20. Optical extinction as a function of wavelength for differing toping levels of tin and the concentric shell model of the resulting ITO nanoparticle [64].

The conductivity experiments showed much higher carrier concentrations in samples with significant levels of Sn surface segregation. The study found good agreement between the Drude model and the experimental results suggesting their theory of nanoparticle Sn surface segregation is the primary cause for their observations. ITO is very good at absorbing wavelengths in the infrared range. Combining ITO nanoparticles with niobate glass produces a material that has an extended range of frequencies it can absorb. This material produces an amorphous thin-film that is able to absorb light in both the infrared and visible range and do so selectively as a function of voltage [5]. This material is able to transition between three states: transparent when 4V is applied, blocking in the infrared range when between 1.5V and 4V is applied, and blocking in both the infrared and visible ranges when less than 1.5V is applied. These three points are obviously generalized, but the study's data shows various concentration levels of ITO nanoparticles compared against baselines of pure niobate glass and ITO nanoparticle thin film. There is a little bit of a tradeoff in the concentration levels where the absorbance of the ITO decreases but the absorbance of the niobate glass increases as more the ITO concentration levels reach the 30% to 50% range [5]. The combination of the two results in a material that is slightly less effective at absorbing infrared wavelengths but significant more effective at

absorbing visible wavelengths. From a light guide and device feature size perspective this is good since the higher the wavelength the smaller the feature sizes can be.
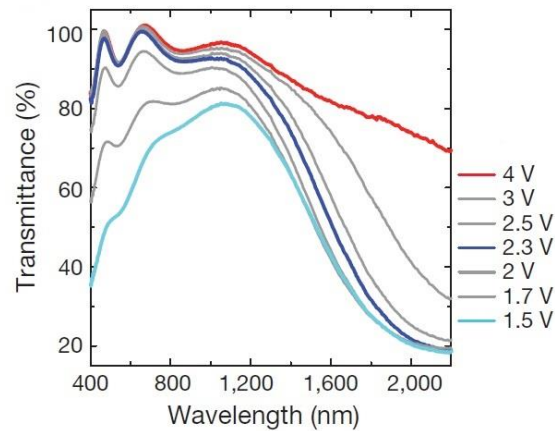
Figure 21. ITO/NbO$_x$ (34% ITO nanoparticles) transmittance at different voltages [5].

Sub-wavelength Light Guides

A light guide is a structure that confines light along a path, for example a fiber optic cable. The principle at play is something called total internal reflection. When light hits an interface between two materials a portion of the light is reflected back and a portion of the light is refracted. The angle of this refraction is given by the relationship between the two material's index of refraction called Snell's law. When this angle becomes extreme enough the light that is bent is essentially bent back into the original material, called total internal reflection. This view of a light guide is one that considers light as a ray. When the angle of the light ray hitting the interface is such that total internal reflection happens, it is said that all of the light stays in the original material. The inner material of a light guide is called the core and the outer material is called the cladding. By choosing the materials correctly, most of the light traveling down the light guide stays in the core. In reality, the light doesn't stop exactly at the interface but rather extends out into the adjacent material in a field that exponentially decays called an evanescent field. Usually the dimensions of the light guide is chosen such that this portion can be ignored. Another aspect of light guides that is ignored in ray theory is diffraction. When a field passes through a smaller and smaller opening or when the dimensions of a material transition become small compared to the wavelength, the field will disperse out more and

more. For example a fiber with a core diameter of 8μm and a cladding diameter of 125μm operating at wavelength of 1250nm has a core that is a little over 6 times larger and cladding that is 100 times larger than the wavelength of the light traveling through it. This mitigates the effects of diffraction and ensures plenty of space between adjacent cores thus negating the effects of the evanescent field and ensuring most of the power stays in the core. An additional mitigating factor for fiber optic cables is the distance between the inputs and outputs. Having these relatively far from each other means that any light that diffracts probably won't make it to a sensor or another interface. Because of these size constraints, fiber optic switching centers in communication networks can be quite large. To move such things to more compact systems, sub-wavelength light guides need to be considered. In such systems, the evanescent field must be considered since it doesn't necessarily get smaller when feature sizes are reduced so it becomes very large with respect to the diameter of the light guide. In the example of a silica core fiber at subwavelength diameters, it can be shown the power is no longer mostly confined to the core as it is in a normal scaled fiber. A significant amount of power exists as the evanescent field outside the core [65]. This example also illustrates how the evanescent field's effects appear to scale up with respect to the core as the core scales down. For 633nm light in 400nm and 200nm diameter cores the power of the evanescent field dissipates to negligible levels near a radius of 500nm in both examples though it gets there much quicker comparatively [65]. In addition to subwavelength fibers, waveguides can be created using periodic structures. The simplest physical structure is a periodic waveguide consisting of rectangles spaced evenly apart [66].
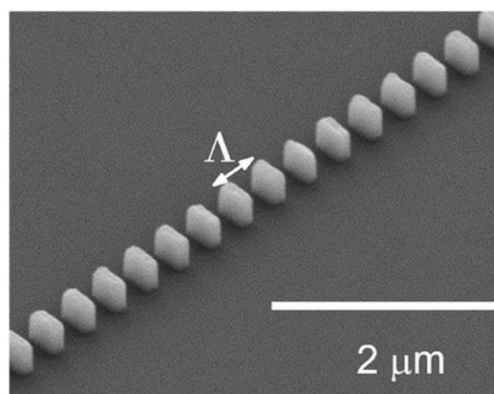
Figure 22. SEM image of a sub-wavelength grating [66].

This type of structure is a diffraction grating. The theory behind it is quantum mechanics. When large numbers of photons are sent through a structure, then classical physics generally describe what happens (whether ray theory or wave theory). Quantum mechanics looks at it as a set of probabilities and these probabilities have a spatial dependence. Macro structures exist effectively as the summation of all the different spatially dependent probabilities where the probabilities of the odd outcomes cancel each other out resulting in the classical result being the only one that is observable. Removing the waveguide material at specific locations relative to the wavelength of the wave results in either reinforcing the probabilities of classical results or removing some aspect of them [67]. In the case of the rectangular subwavelength grating (SWG) the exact dimensions can allow the structure to operating in several different regimes: diffraction, reflection, and subwavelength. The diffraction regime scatters an incoming beam in different orders, the reflection regime is able to reflect an incoming beam backwards, and the subwavelength regime allows for the suppression of diffraction effects [66]. For light guides like SWGs, metal is the preferred material since the surface plasmon resonance is well studied and the properties of which can be controlled through particle/structure dimensions. As was previously stated, metals are not the only materials to exhibit surface plasmon resonance. Technically anything with free charge carriers can be used like semiconductors [50]. In addition to this, it was been theoretically demonstrated that dielectric materials with sufficiently high permittivity can also be used as subwavelength light guides. It should be noted that this permittivity is very high, needing to be greater than 14. The study does note that Silicon-Germanium in the proper molar ratio has a permittivity that is high enough in the real part while the imaginary part is low enough to significantly reduce losses [68]. The main point of using a high permittivity material is to reduce the losses from 0.2dB per 100nm (0.6dB per 100nm actual) to a theoretical 0.01dB per 100nm. Nanoscale light guides were simulated using spherical particles with radii of 50nm and spaced 150nm apart showing good confinement of the light and even the ability to create Y-splitters and angled elbow paths. Where these light guides changed direction or split, there were higher losses predicted in the simulations of -2.9dB for the Y-splitter and -5dB for the angled elbow [68].
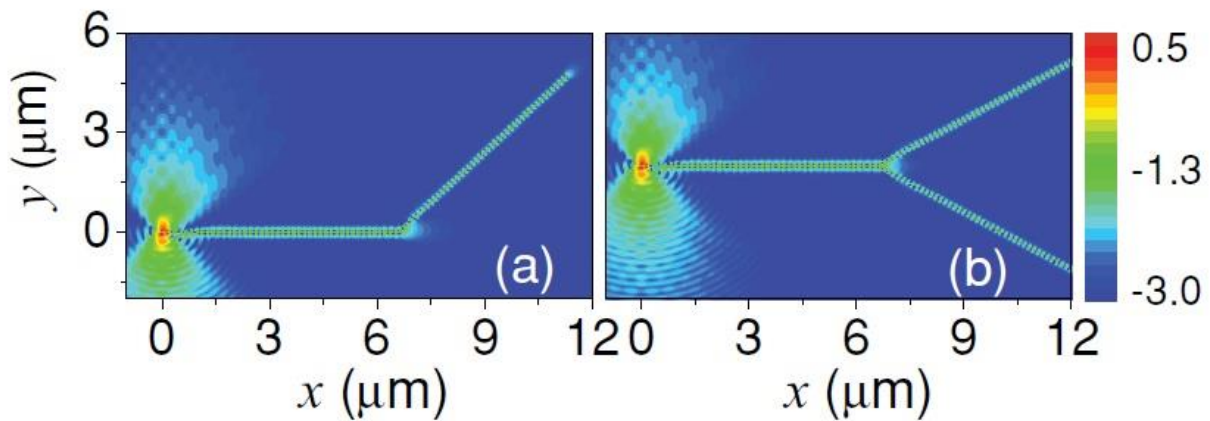
Figure 23. Simulations of a Si-Ge subwavelength grating elbow and Y-splitter [68].

Similar in physical structure to the SWG waveguide is a metal-dielectric-metal (MDM) waveguide with side coupled resonators [69].
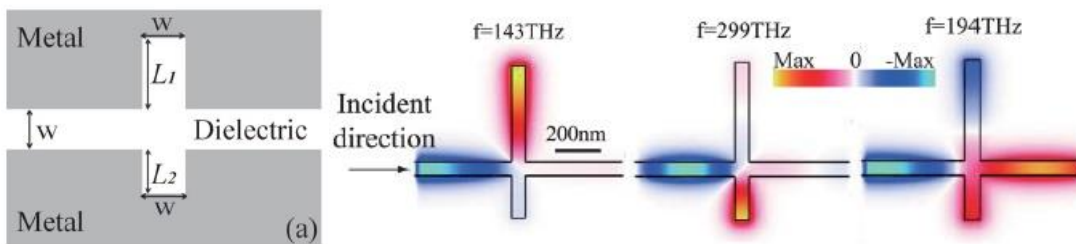
Figure 24. Metal-dielectric-metal side coupled wave guide [69].

In this regime, there is a very narrow path made up of dielectric material with metal on either side. Periodically, there are cavities on either side of the path of the same width as the main dielectric path. The lengths of these cavities are not the same on both sides of the path, but they are located at the same points along the path's length. The asymmetry of the cavities leads to the light guide taking on behavior similar to electromagnetically induced transparency. The difference between the two side's cavity lengths directly correlates to the bandwidth of the transparency window: as the difference between the cavity lengths increases, the width of the transparency window increase. Simulations then show an inverse relationship between the cavity length difference and the group velocity of the light traveling through the structure which is expected behavior for electromagnetically

induces transparency [69]. The study also shows the correlation between the periodicity of the cavity spacing to center frequency of the transparency window. As the distance between the cavities decreases, the transparency window shifts higher in frequency but also shows a greater bandwidth. This is attributed to coupling between adjacent cavities. The closer the cavities are to one another, the greater the coupling between them is [69]. A different cavity based MDM structure is numerically demonstrated by placing two Ag plates very close together (10nm to 40nm) and using low ridges to form the light guide itself and a very small diameter hole acting as the input [70]. This structure relies on surface plasmon polaritons for the actual transport of energy and was shown to be able to confine light to a cross-sectional area of 10nm x 20nm over a distance of 10μm. This structure consisted of a single hole in the bottom Ag plate with a diameter of about 20nm (that dimension isn't specifically noted in the study) with a 20nm tall, 10nm wide ridge protruding from either side out 5μm in either direction. The distance between the top of the ridge and the upper Ag plate was fixed at 10nm. Simulations where run on light with wavelength of 1300nm with the ridge height set to 20nm and 30nm which corresponds to a distance between the Ag plates of 30nm and 40nm respectively. This showed surface plasmon polariton wavelengths of 740nm and 769nm respectively but most importantly, showed that 40nm Ag plate separation results in extremely good confinement of light. This demonstrated some dependence on the distance between the Ag plates. The closer the plates were places to one another, there is a shift to larger wave vectors for the same wavelength. This distance is independent of the height of the ridges and can serve as an additional parameter that can be tweaked in design. By red shifting the surface plasmon polariton 29nm they achieved a roughly 39% increase in signal isolation between adjacent light guides (estimated from the graphical simulation results) [70].
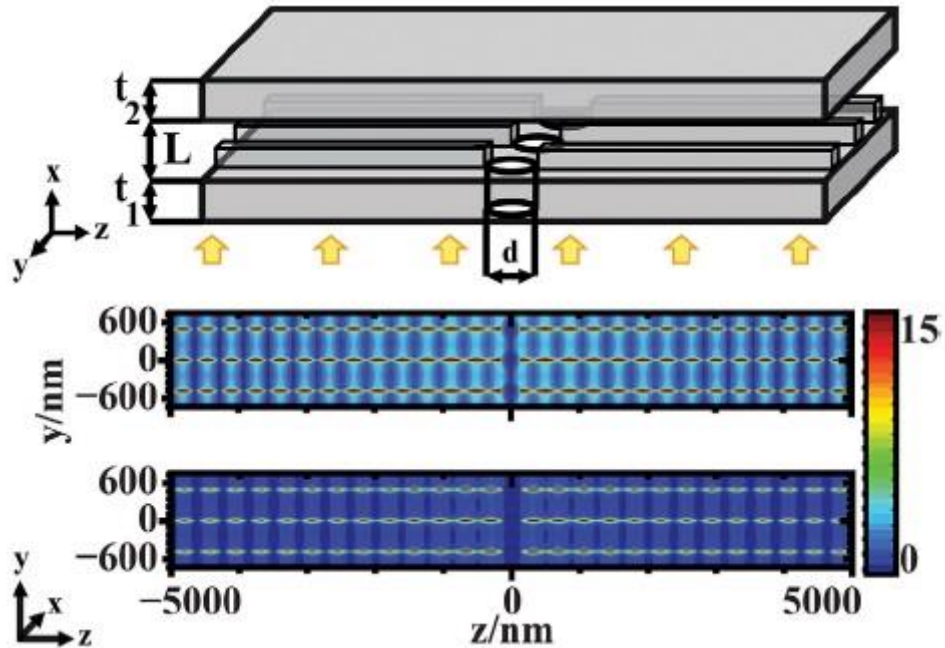
Figure 25. Aluminum cavity wave guide showing the electric fields for two different spacings of L = 30nm (top) and L = 40nm (bottom) while keeping the ridge to upper plate gap constant at 10nm and a wavelength of 1300nm [70].

Similar to a MDM waveguide is a multi-layered plasmon-dielectric hybrid system. This is a relatively simple structure of multiple dielectric layers whose permittivities and thicknesses are chosen such that the high order frequency based dispersion is effectively eliminated [71]. The concept is to start with a simple metal-dielectric structure. Then, between the dielectric and the metal another layer of a different dielectric is placed with a higher permittivity. Additional layers of dielectric can be placed at the bottom of the stack but this time with permittivities incrementally smaller than the layer on top of it (and decreasing thicknesses).
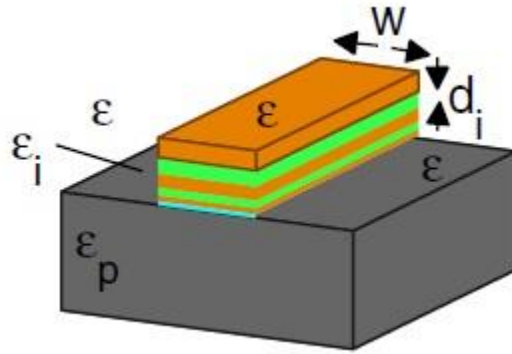
Figure 26. Wave guide with layered dielectrics [71].

On the side with metal, the surface plasmon polariton is confined to the metal-dielectric interface but on the dielectric side, it is able to extend relatively far into the dielectric. For small wave vectors, the surface plasmon polariton extends very far into the dielectric effectively seeing only the outer most material binding the surface plasmon polariton to the interaction between the metal and that layer of the dielectric. For very large wave vectors, the surface plasmon polariton to the next layer and so on incrementally down to the physically closest dielectric layer. For small wave vectors, the behavior is mostly unchanged, but for higher order wave vectors the inner layers begin to dominate the response. If the permittivities and thicknesses are chosen correctly, a structure can be theoretically created that allows for slow and subwavelength propagation of short pulses with no phase or amplitude distortion [71]. A somewhat similar, though geometrically more complex and metamaterial dependent, approach to managing light at the subwavelength scale is given in a set of simulations described as subwavelength ray optics. By carefully managing dispersion throughout the path of the light, the study claims to be able to guide light at diameters of $\lambda/10$ with spacing of $\lambda/5$ along curved paths using metamaterials [72]. This is done by doing a conformal transform of three-dimensional space to get an equivalent two-dimensional space. Metamaterials are then alternated with their physical design being defined in the transformed two-dimensional space. A simulation was performed using alternating curved layers of Ag and GaN with curves defined in their equivalent two-dimensional space though it should be noted that no actual experiments were performed and fabrication methods would be extraordinarily difficult. However difficult the fabrication might be, the paper does show through

simulation an interesting reduction of both diffraction and evanescent fields [72]. On the other hand, a different study showed good experimental data demonstrating good light confinement of a sub-wavelength light guide. A set of light guides made from TiO_2 on glass were imaged using photon scanning tunneling microscopy (PSTM) to gather the spatial distribution of electric field intensity in subwavelength light guides [73]. The glass used was BK7 (alkali-lime silicates with 10% potassium oxide) with a refractive index of about 1.515. TiO_2 was chosen because its dielectric function of 5.3 is higher than the glass which helps offset problems with coupling the incident light as the light guide cross-section gets smaller. Using standard electron beam lithography and reactive ion etching, 200nm wide, 150nm high, 40μm long light guides made form TiO_2 were formed atop the BK7 glass substrate. Spacing was chosen to be 20μm between adjacent light guides to make sure there was no cross-talk between them. The incident light was provided by a He-Ne laser with a wavelength of about 633nm. PSTM measurements were obtained using a fiber tipped with 7nm of Cr to shield the tip from scattered light. Electric field intensities were obtain with PSTM at a constant height yielding a spatial distribution of the field intensities. Using this method allows for accurate mapping of the light confinement in the guide since power measurements require both electric and magnetic field measurements to be obtained simultaneously which the Heisenberg uncertainty principle forbids. The probe was placed about 350nm above the top of the light guides (500nm above the substrate).
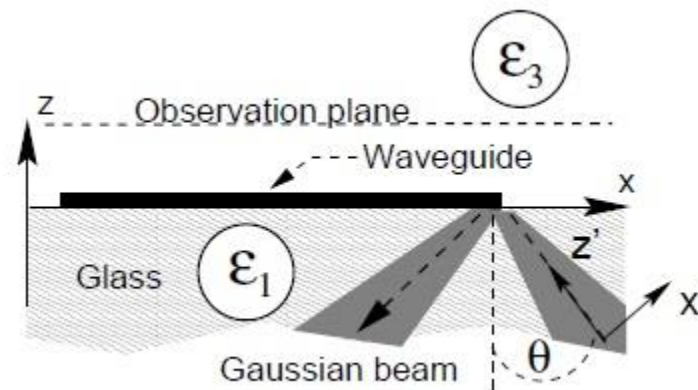
Figure 27. Observation method for measuring the light confinement of the TiO_2 light guide [73].
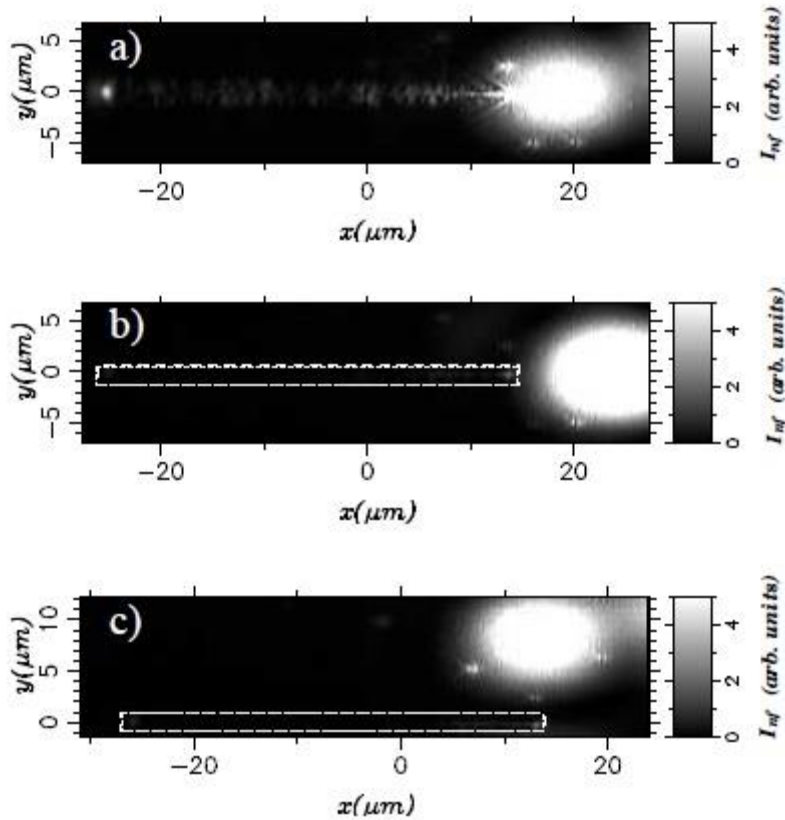
Figure 28. Measurements of the TiO₂ light guide with the incident beam entering the light guide (a) and with it hitting other areas of the substrate (b) and (c) to confirm the observed light was in fact traveling through the light guide and not some other effect [73].

Observing the entire guide including the incident light source resulted in an a scale for the amplitude that made the guided light difficult to distinguish from the incident light; however even in this scaling both the light at the exit of the guide and the guided light were still visible. The incident light was then tested at to other locations relative to the entrance of the light guide showing a lack of coupling which would be expected. The successful capturing and guiding of light with a properly oriented incident light sources was reproduced on over 30 other light guides on the test substrate. To get better resolution on the light confinement in the light guide, five PSTM images covering a 5µm by 5µm area at a probe height of 10nm to 50nm were stitched together. This imaging showed good light confinement to a width of roughly 300nm (given the TiO₂ widths were 200nm).
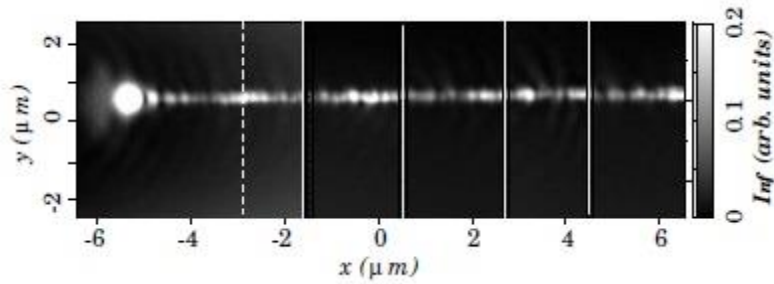
Figure 29. High magnification stitched image showing the measured light confinement in the light guide [73].

A comparison of the measured and numerically predicted electric field intensities was done showing nearly a nearly identical normalized intensity profile with respect to the light guide's width. The very small differences noted are attributed to TiO_2 roughness leading to scattering. The numerical result was obtained using Green's dyadic method to compute the electromagnetic near-field distribution in a plane parallel to the sample surface, though the sample length in the simulation was reduced to 10μm to keep calculation times reasonable [73].
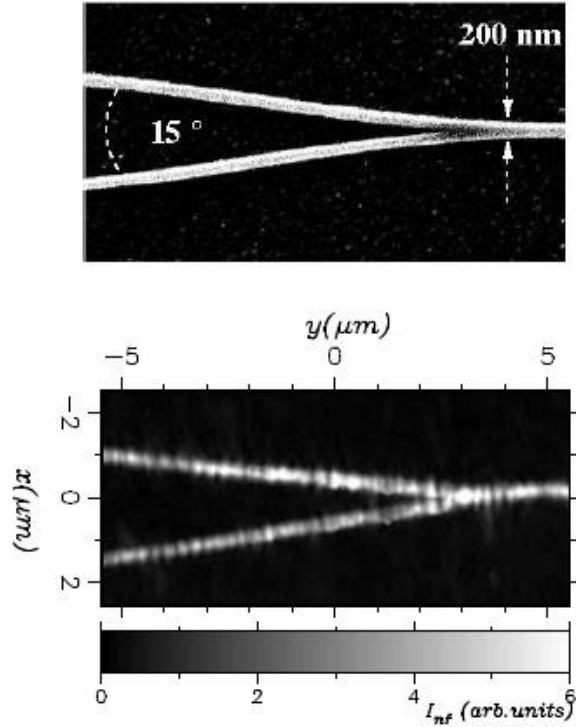
Figure 30. SEM image of a TiO_2 Y-splitter (top) and imaging of the measured light confinement (bottom) [73].

Literature Review Summary

There is promising research in the area of plasmonics making subwavelength light guides appear like a plausible way of creating integrated photonic circuits. History suggests the idea of a fully integrated photonic circuit that can compete with Si-based integrated circuits is not a feasible one. It would be advantageous to find an application that would make the two complimentary. While light-based switching has obvious practical applications in the telecommunications industry, it is possible that such similar switching code meet a need in the field of integrated circuits. We are exceedingly good at making 2D structures in Si wafers, but moving effectively into the 3rd dimension has proved difficult. Finding a method to add another type of switch on-top of existing Si-based wafer technologies would provide a possible alternative avenue to achieving some 3D integrated circuit designs without the need for SOI or bonding wafers together. This thesis examines a potential technology.

This idea is to create a switchable photonic trace that can be created using existing wafer processes that can be built up on top of Si-based wafers. The switchable photonic trace uses a material that whose transmittance can be changed by applying an electric field. Since generally such a material is also conductive and an electric field is needed to produce the switching effect, a simple parallel plate capacitor makes a convenient structure to base the switch off of. One plate is proposed to be the switchable optical material with a dielectric surrounding it on all sides with a lower refractive index to satisfy total internal reflection. Then a layer of metal is proposed to run parallel to the switchable material. Charging the capacitor would apply an electric field causing a transmittance change and discharging the capacitor would remove the electric field producing the opposite transmittance effect.
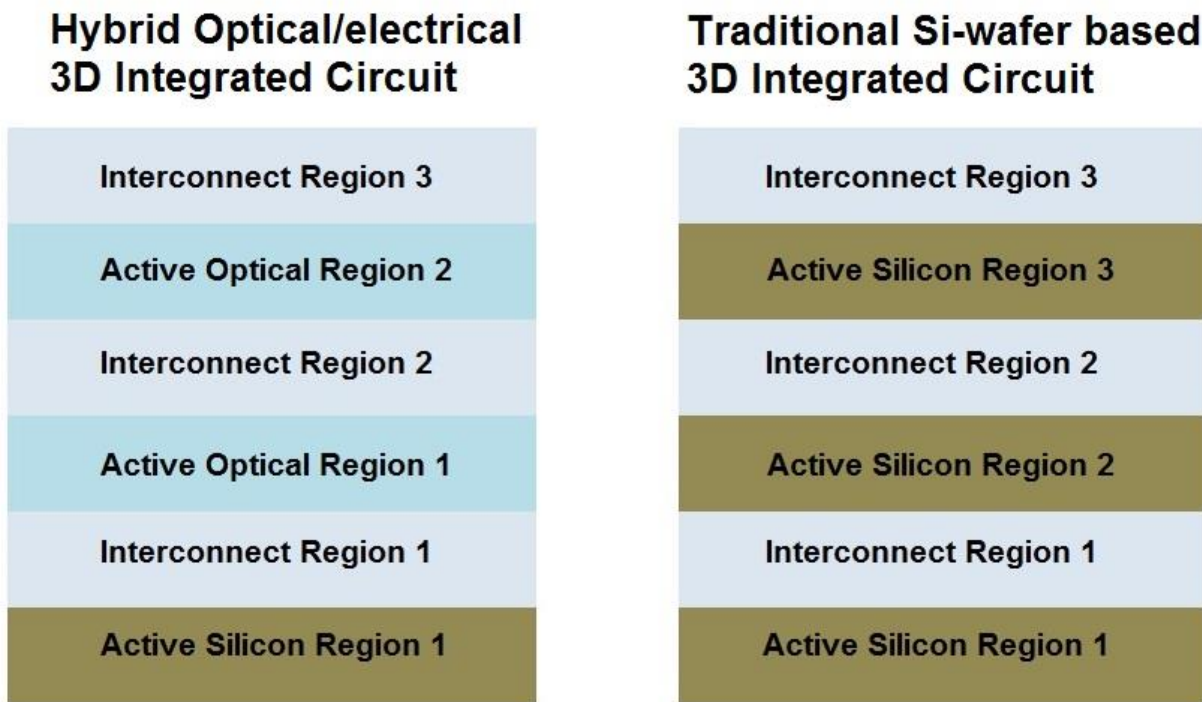
Figure 31. Comparison of proposed optical switch on Si wafer 3D IC versus a traditional wafer-on-wafer structure.
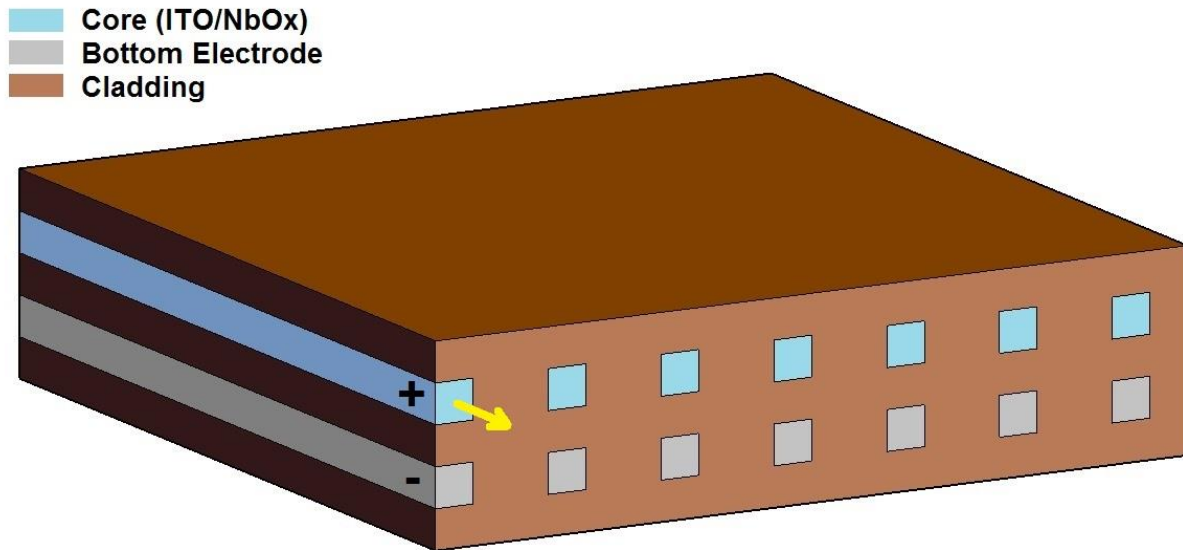
Figure 32. Concept drawing of a capacitor based optical absorption switch.

To fully realize such a device, a number of problems will need to be solved. Since the proposed switch is an optical effect that is controlled by an electrical effect and because the switch is proposed to function in a complimentary fashion to Si-based wafers, optical/electrical conversion will be something that needs to be addressed. This takes the form of two problems: Light generation/distribution and light sensing. Additionally device properties will need to be addressed such as switch core/cladding materials, switch length, and minimum distance between adjacent switches. Finally the proposed structure and materials will need to be compatible with traditional Si-based wafer technology. The scope of this thesis is to evaluate a specific material as the switchable material: ITO/NbO$_x$ [5]. It will be evaluated in conjunction with three potential cladding materials (SiO$_2$, Teflon AF 1601, and nanoporous silica) at two wavelengths (475nm and 1.55μm). The other plate of the proposed capacitive structure is suggested to be Aluminum because of it prevalent use as integrated circuit metal lines. This will address two of the three main problems that need to be solved to make this technology viable: device structure and compatibility with Si processes. The problem of light generation, distribution, and sensing is not within the scope of this thesis; however it should be noted that the wavelengths chosen for simulations were chosen such that LEDs can produce them. 1.55μm

was chosen because of its usage and existing technology related to fiber optic communications and 475nm was chosen because it is near the wavelength of blue LEDs. Additionally there is research demonstrating diffraction gratings being used to get light into subwavelength light guides and this effect works at right angles. Shining light on a diffraction grating from above makes the light move out in-line with the grating path.

CHAPTER 3 TASKS

ITO/NbO$_x$ Material Evaluation for use as the Core

Significance: Determine the necessary parameters of a light guide consisting of ITO/NbO$_x$ as the core material for 475nm and 1.55µm wavelengths to run simulations

Method: Literature Review and Simulation

Results:

ITO/NbO$_x$ is a material that is switchable in both infrared and visible wavelengths. This material was reported in as a thin-film in a Nature Letter for selectively switching infrared and visible sunlight. It is made up of ITO nanoparticles ranging between 5nm and 15nm that are processed with hexaniobates. The ITO portion of the material is responsible for the switch-ability in the infrared range and the NbO$_x$ is responsible for the switch-ability in the visible range. By bonding the ITO nanoparticles to the NbO$_x$ the researchers describe the ITO and NbO$_x$ sort of merging together producing a material with different properties than either of the original constituents. By trading off some of the ITO's infrared light switching performance, the visible light switching performance increased significantly [5]. Because this is not a traditional material with well-defined material properties, it was necessary to extrapolate the necessary properties from what has been reported thus far. The first task was determining the percentage ITO and NbO$_x$. The ITO gets bonded to hexaniobates and then to alter the exact properties the researchers added this bonded ITO/NbO$_x$ to a solution of decaniobates. By altering this percentage they were able to get differing transmittance switching profiles. Examining these profiles at the two wavelengths of 475nm and 1.55µm it was determined that for 475nm an ITO concentration of 34% and for 1.55µm an ITO concentration of 69% provide the best switching performance. The basis of which was the greatest contrast between the minimum and maximum transmittance combined with a reasonable maximum transmittance as to avoid unnecessary losses. These transmittance profiles were measured through a thin-film 150nm thick. For the sake of simplicity, a switch that is absorbing light will be said to be in an ON state and a switch that is allowing light to pass will be said to be an OFF state. From the transmittance profiles the following was determined:

Wavelength	ITO Concentration	ON (150nm)	OFF (150nm)	ON (1nm)	OFF(1nm)
475nm	34%	43%	90%	99.44%	99.93%
1.55µm	69%	35%	85%	99.30%	99.89%

Table 1. Transmittance [5].

These numbers pulled from graphs are the transmittance through 150nm of material. To determine the transmittance per nanometer the transmittance through 300nm of material was calculated representing two units of 150nm in series.

$$(0.43)(0.43) = (0.43)^2 = 0.185$$

This answer was then used to solve for the transmittance per nanometer where each unit is 1nm, then 0.185 represents the transmittance of 300 units in series.

$$X^{300} = 0.185$$

$$X = (0.185)^{1/300}$$

$$X = 0.9944$$

For the sake of clarity, from here out the ITO/NbO$_x$ mix consisting of 34% ITO nanoparticles will be referred to as ITO34 and an ITO/NbO$_x$ mix consisting of 69% ITO will be referred to as ITO69.

Next it was necessary to determine the refractive index of each material at the desired wavelengths. Unfortunately there isn't any information available for this material regarding refractive index since this isn't a particularly important parameter for switching in a thin-film form, but is critical to a light guide. To determine this, the refractive indices for ITO nanoparticles and niobate glass were looked up in literature then were combined to estimate the refractive index of ITO/NbO$_x$. Refractive index describes how light travels through a medium referenced to how it would travel through a vacuum. Effectively this is the speed of light through a medium. Since ITO/NbO$_x$ consists of part ITO nanoparticles and part niobate glass, it could be reasoned that the light will travel some distance through ITO nanoparticles and some distance through niobate glass for a given length through the material. The amount of each would be proportional to the percentage of the material made of up of each material. It can be reasonably estimated that light traveling through ITO34 would travel through ITO nanoparticles for 34% of the material and niobate glass through the rest. While the refractive

index of bulk ITO is a well-studied parameter it is significantly different than ITO nanoparticles. For

example, at 475nm bulk ITO has a refractive index of about 2 while simulations shows that ITO

nanoparticles having something closer to 1.5 [74, 75]. For the NbO$_x$, the bulk properties were used

since ITO/NbO$_x$ effectively uses NbO$_x$ as the bulk material with ITO nanoparticles suspended in it which

has a refractive index around the 2.2 to 2.4 range [76]. The differences between bulk ITO and ITO

nanoparticles show that smaller structures of a given material may have lower refractive indices than

their bulk counterparts. This effect is not considered for the NbO$_x$ but it is likely there is some

reduction of the refractive index for the hexaniobates that are bonded to the ITO nanoparticles. This

would mean some portion of the NbO$_x$ will be both a structure on the nano scale and be somewhat

altered due to the presence of the ITO it is bonded to. To estimate the overall refractive index of a

given concentration of ITO/NbO$_x$ the following formula was used where *ITO%* is the fraction ITO

nanoparticles in the material. From this equation refractive indices for ITO34 at 475nm and ITO69 at

1.55µm where estimated where ITO34 was the optimal ITO concentration chosen for switching at

475nm and ITO69 was the optimal ITO concentration chosen for switching at 1.55µm.

$$(ITO\%)n_{ITOnano} + (1 - ITO\%)n_{NbOx} = n_{ITO\%}$$

Wavelength	ITO Concentration	Refractive Index
475nm	34%	2.1181
1.55µm	69%	1.4521

Table 2. ITO/NbO$_x$ Refractive Index [75, 76].

The proposed dimensions of each switch depends on the transmittance of a given ITO concentration at

a given wavelength. Since the transmittance profile actually depends on the concentration of ITO

nanoparticles, it was decided to examine the effects of non-uniformity on the ITO concentration. At

very small dimensions having one too many or one too few nanoparticles would have a significant

impact the transmittance properties of that particular switch. The following analysis looks at the

cross-sectional areas showing the error in ITO concentration as a function of area to get an idea of the

relationship.
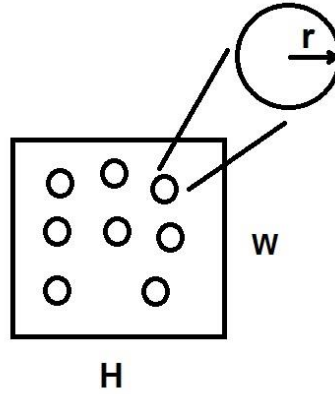
Figure 33. Cross-section and Nanoparticles.

The number of nanoparticles needed to create the same ratio of materials as ITO% given a nanoparticle radius r and wave guide height H and width W is given by the following equation. Assuming a maximum diameter of 15nm the following table shows the expected window for concentration error assuming whole numbers of nanoparticles. For example in a 100nm by 100nm light guide 4.81 nanoparticles are needed to create the proper 34% ITO concentration. Having only 4 results in a nearly 17% error and having 5 results in a 4% error. It should be noted this effect might be avoidable due to etching, but the effects of partial nano-particles in a very small structure is not known at this time.

$$ITO\% \left(\frac{HL}{\pi r^2}\right) = N_{np}$$

ITO%	H (nm)	W (nm)	r (nm)	n	Error (+%)	Error (-%)	Error Range
34	100	100	15	4.810016	16.84%	-3.95%	20.79%
34	100	200	15	9.620032	6.45%	-3.95%	10.39%
34	100	300	15	14.43005	2.98%	-3.95%	6.93%
34	100	400	15	19.24006	1.25%	-3.95%	5.20%
34	100	500	15	24.05008	0.21%	-3.95%	4.16%
34	**200**	**200**	**15**	**19.24006**	**1.25%**	**-3.95%**	**5.20%**
34	200	300	15	28.8601	2.98%	-0.48%	3.46%
34	200	400	15	38.48013	1.25%	-1.35%	2.60%
34	200	500	15	48.10016	0.21%	-1.87%	2.08%
34	200	600	15	57.72019	1.25%	-0.48%	1.73%
69	100	100	15	9.761503	7.80%	-2.44%	10.24%
69	100	200	15	19.52301	2.68%	-2.44%	5.12%
69	100	300	15	29.28451	0.97%	-2.44%	3.41%
69	100	400	15	39.04601	0.12%	-2.44%	2.56%
69	100	500	15	48.80752	1.65%	-0.39%	2.05%
69	**200**	**200**	**15**	**39.04601**	**0.12%**	**-2.44%**	**2.56%**
69	200	300	15	58.56902	0.97%	-0.74%	1.71%
69	200	400	15	78.09203	0.12%	-1.16%	1.28%
69	200	500	15	97.61503	0.63%	-0.39%	1.02%
69	200	600	15	117.138	0.12%	-0.74%	0.85%

Table 3. Cross-sectional area comparison

The actual length of each switch was determined using the per-nanometer ON/OFF transmittances. A balancing act is required here to provide the most difference between ON/OFF states while still maintaining reasonable transmittance in the OFF state.

ITO%	Length (nm)	ON (T)	OFF (T)	ON/OFF Diff
34	100	0.570311	0.932371	0.362060209
34	200	0.325254	0.869316	0.544061258
34	300	0.185496	0.810525	0.625028582
34	**400**	**0.10579**	**0.75571**	**0.649919245**
69	100	0.495364	0.89578	0.400415434
69	200	0.245386	0.802422	0.557035674
69	300	0.121555	0.718793	0.597237683
69	**400**	**0.060214**	**0.64388**	**0.583666203**

Table 4. Transmittance versus length.

A trade-off in the dimensions was accepted for this thesis. A wider light guide provides for less susceptibility to ITO concentration non-uniformities as demonstrated above. Additionally, the length of each switch is likely best at shorter distances because of better transmittance in the OFF state and less overall absorption. The height and width of 200nm and the length of 400nm was chosen as a compromise between performance and shape. Since the method of simulation run below assumes a light guide which is very long, actually simulating a switch that was longer than it was wide made for a more meaningful result. If changing the shape of the guide that drastically results in effects not captured in the simulation, then hopefully the chosen shape mitigates those effects.

Baseline Simulation of a Square ITO/NbO$_x$ Light Guide

Significance: Get a baseline for how much light needs to be dealt with between adjacent light guides. Will be used to help evaluate how densely populated the device can be while avoiding cross talk.

Method: Simulation

Results:

These are the baseline simulations of ITO34 and ITO69 fully surrounded by air. The purpose of these simulations was to gain insight into the scales that will need to be considered at each ITO concentration level and wavelength and any potential issues that would prevent the material from functioning as a light guide. To run simulations for this thesis, the Matlab implementation of the extended Marcatili approach for rectangular light guides was used [77]. This method was chosen in part because of its ability to more accurately model rectangular light guides with high refractive index-contrasts. This allows the same tool to be used to model very small scale structures which generally only function with high refractive index-contrasts. For reference, fiber optic cables using silica cores have refractive indices around 1.5 and are considered low contrast compared to silicon having an index around 3 which is considered high contrast. ITO34 falls somewhere between with an index of around 2 and ITO 69 is about 1.46 which is worse than a normal fiber optic cable (at 1.55μm). By using the extended Marcatili method it can be reasonably assumed the plots of ITO34 should be fairly accurate since it is lower than silicon. This method is also used to model small rectangular silicon light guides meaning again modeling the ITO34 and ITO69 light guides a small dimensions should provide reasonably

accurate results. Both light guides were simulated at the same dimensions of 200nm by 200nm. This

simulation method uses five regions: the core defined as region 1 and four surrounding regions 2-5

defining the surrounding materials. The regions are only defined for each of the directions primary

axes x and y (i.e. no results are calculated for the diagonals since enough information is gathered from

the primary axes making the diagonals either redundant or unnecessary). The z-axis is defined to be

the direction of propagation of the light. To simplify the code this simulation just changes the

orientation of the light guide to solve for the y-axis information. This is done so that only code solving

for the x-axis has to be written. Figure (a) shows the orientation of the light guide, (b) be shows the

profile, (c) and (d) show how the light guide is rotated during simulation to cut done on the code they

needed to write, and finally (b) illustrates the lack of solving for the diagonals.
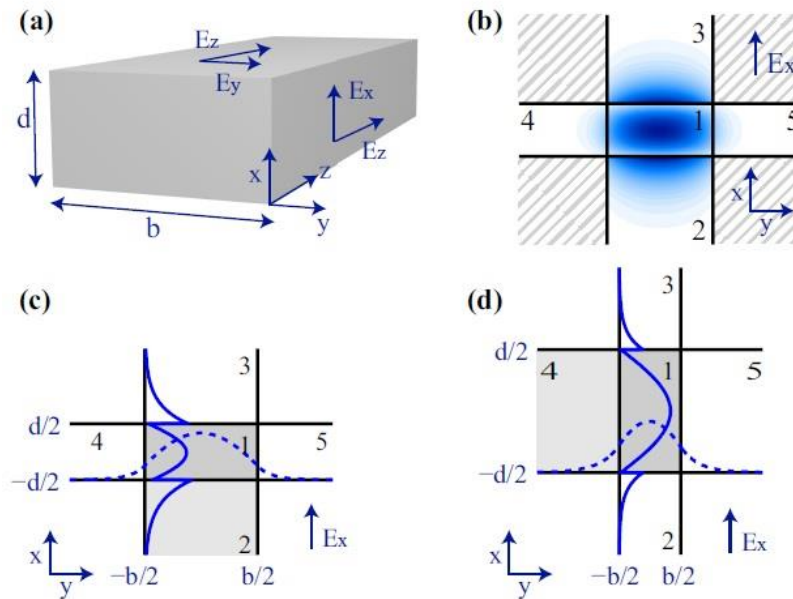
Figure 34. Axis definitions for Matlab implementation of the extended Marcatili approach for
rectangular light guides [77].

Making the length and width the same further simplifies the final product. The baseline simulations

were run as follows:

Wavelength	Width	Height	Core	n1(core)	Substrate	n2(sub)	Dielectric	n3-5(delectric)
475nm	200nm	200nm	ITO34	2.1181	Air	1	Air	1
1.55µm	200nm	200nm	ITO69	1.4521	Air	1	Air	1

Table 5. Baseline simulation set-up.
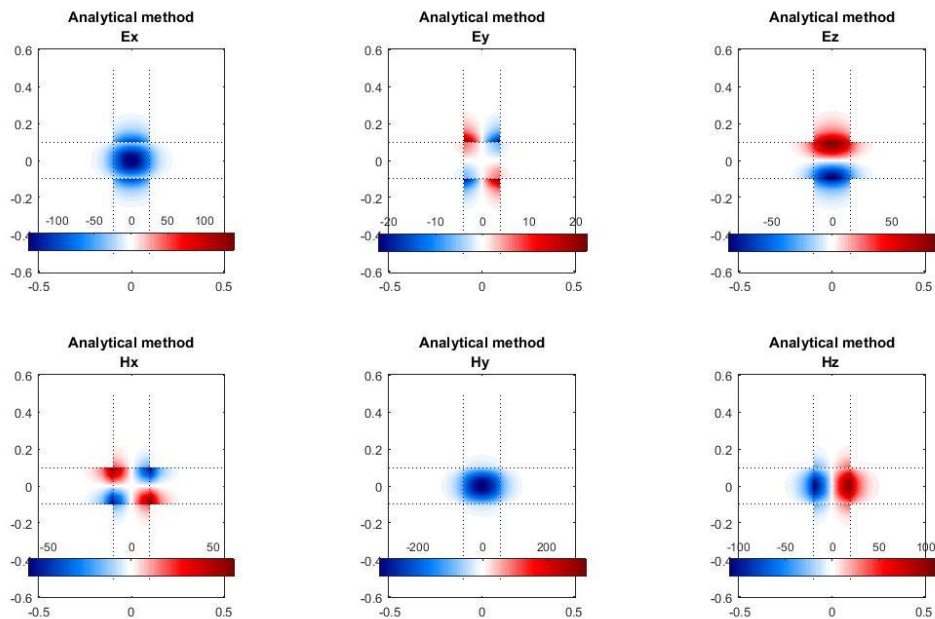
Figure 35. ITO34 at 475nm (x and y axes are in µm)
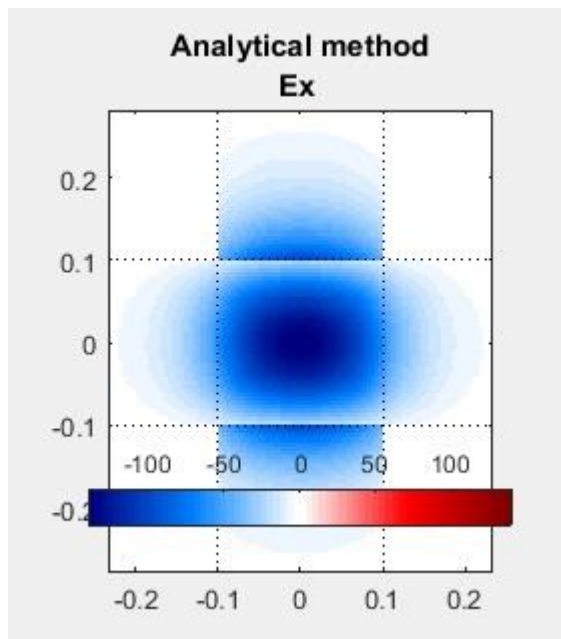
Figure 36. ITO34 at 475nm E_x Zoomed

ITO34 at 475nm shows very good initial results. This shows very good light confinement. The last data point that shows up in the plot occurs at 117.5nm form the edge of the guide for the y-axis (width) and 167.5nm in the x-axis (height). The E_x component of the field is the strongest (which is in part to how the simulation runs). The E_y and E_z components actually extend out farther than the E_x component in the x-axis; however they are 14% and 56% of the intensity of the E_x component making their actual impact significantly less the E_x component. This means the E_x component dominates the distance out from the edge of the light guide the light reaches. This is supported by comparing the absolute limit of each field component to the point at which it is reduced to 10% of the absolute maximum field intensity.

Field (y-axis)	Limit	10%
E_x	117.5nm	67.5nm
E_y	57.5nm	n/a
E_z	127.5nm	52.5nm

Table 6. Field reach from the edge of the light guide in y-axis for ITO34

Field (x-axis)	Limit	10%
E_x	167.5nm	102.5nm
E_y	172.5nm	27.5nm
E_z	177.5nm	87.5nm

Table 7. Field reach from the edge of the light guide in x-axis for ITO34

The x-axis, which represents height, is of the least concern since the proposed structure will have regions of interconnects between each active region, although it is worth noting. The y-axis, which represents the distance between two adjacent switches, is the dimension of primary concern. Placing switches at least 255nm apart will effectively mean that not even the edges of the fields will overlap. Adding to this dimension a guard band would be the safest way to do an initial build of the proposed technology ensuring a minimum amount of cross talk which would be advantageous for any initial testing. The actual switch density would not only be a function of the fields outside of the switches but also the length of the switch (affects the ON/OFF transmittance difference) and optical/electrical converter sensitivity that would need to be at the end of the switch. For the purposes of this thesis, the 10% point was chosen because 10% cross-talk likely would be tolerable. It should be noted that it

may be possible to tolerate more cross talk meaning switch density could be further compressed. Based on this 10% point, the minimum distance between adjacent switches would be 67.5nm for ITO34 surrounded by air. This of course isn't a structure that can be built as a 3D integrated circuit. A dielectric that will not perform as good as air will be needed.
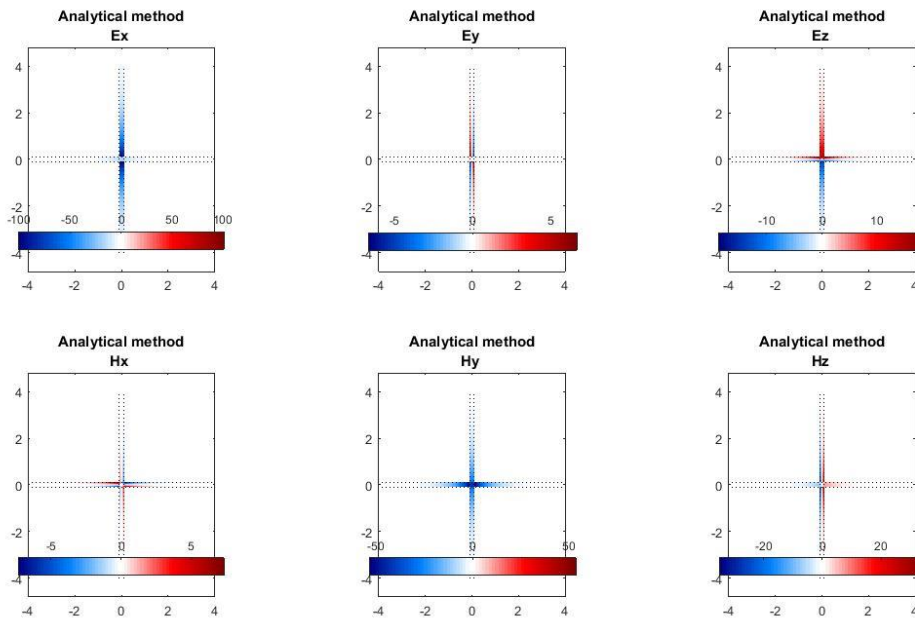
Figure 37. ITO69 at 1.55μm (x and y axes are in μm)
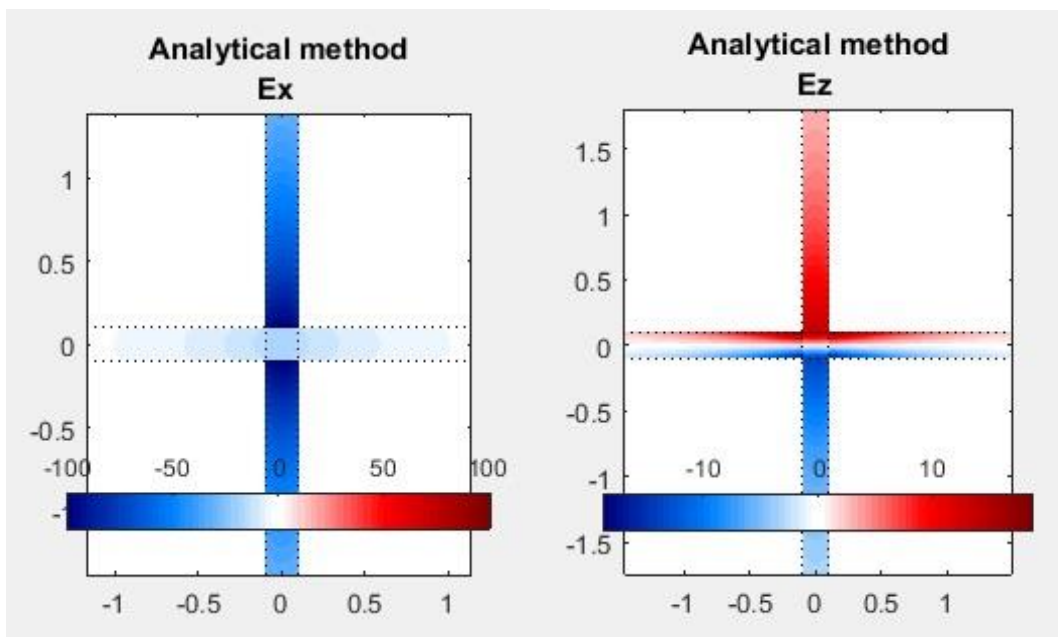
Figure 38. ITO69 at 1.55μm E_x Zoomed   Figure 39. ITO69 at 1.55μm E_z Zoomed

56

The simulation of ITO69 at the nanoscale shows a failure of the switch to support much of anything inside the switch core. The E_x component which is supposed to be the primary component effectively doesn't travel at all inside the switch but rather in the cladding. Changing the dimensions of the light guide from 200nm by 200nm to 1μm by 1μm results in a normal looking light guide response; however a 1μm thickness is not practical. Experimenting shows that in order to support the E_x component inside the switch the thickness needs to be about 500nm. Even at this point the performance is not very good as the intensity inside the switch is 24% less than it is outside. Additionally the intensity of the E_z component of the field is actually comparable to the E_x component. While this is possible, it is not really practical for 3D integrated circuit applications.
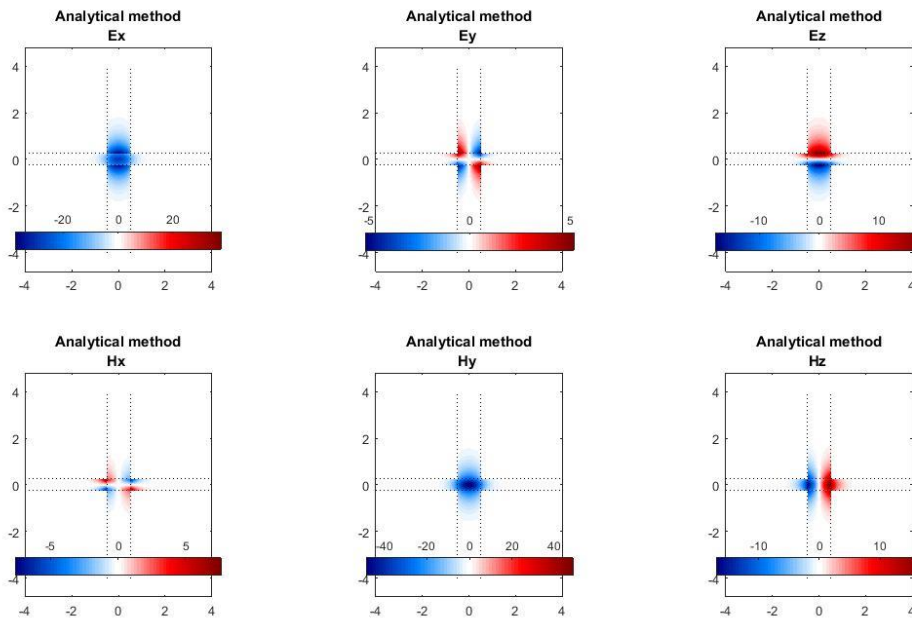
Figure 40. ITO69 at 1.55μm (x and y axes are in μm). Width is 1μm and height is 500nm
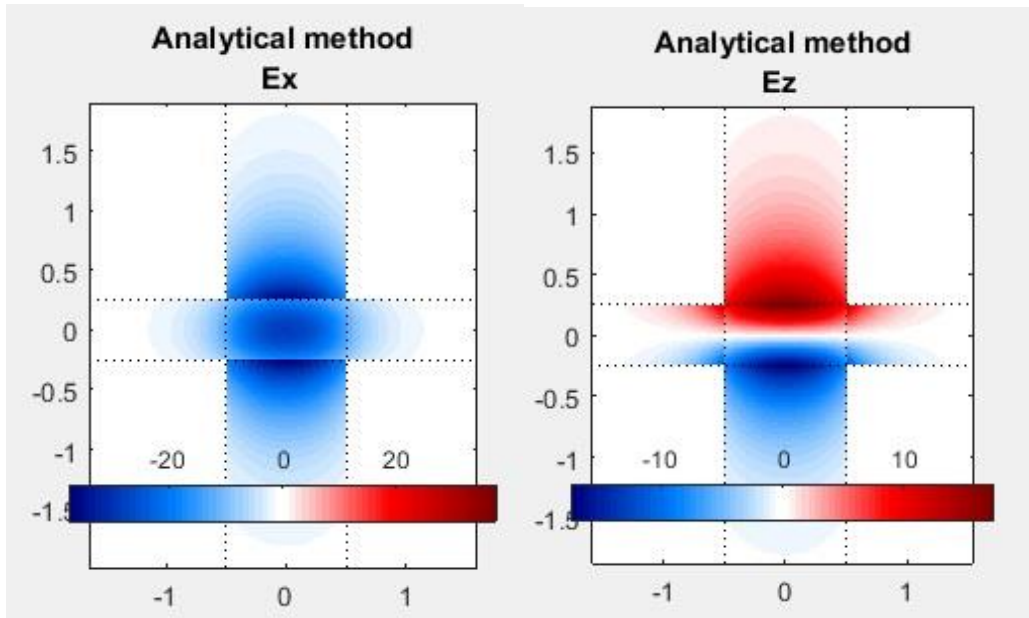
Figure 41. ITO69 at 1.55μm E_x Zoomed (1μm x 500nm)   Figure 42. ITO69 at 1.55μm E_z Zoomed (1μm x 500nm)

Field (y-axis)	Limit	10%
E_x	643nm	343nm
E_y	703nm	n/a
E_z	843nm	303nm

Table 8. Field reach from the edge of the light guide in y-axis for ITO69

Field (x-axis)	Limit	10%
E_x	1567nm	1048nm
E_y	1467nm	223nm
E_z	1528nm	698nm

Table 9. Field reach from the edge of the light guide in x-axis for ITO69

Despite its practical short comings, there can be reasonably good switch density compared to the switch dimensions at 343nm between each switch compared to a 1μm switch width. Looking at the y-axis however shows another problem. There would need to be a minimum of 1μm between layers of ITO/NbO$_x$ which again while not impossible, puts a significant limitation on design of a 3D integrated circuit. None of this takes into consideration that much of this light would be absorbed adding additional heat to the device which is known to cause issues in 3D integrated circuits.

The baseline simulation of ITO34 at 475nm looks very promising showing good light confinement, the ability to quite densely pack switches, and likely little layer to layer concerns. The baseline simulation of ITO69 at 1.55μm shows at the 200nm switch scale it fails to confine light. The dimensions of the switch can be scaled up to produce a potentially functional switch, but its performance is not very good. There are two things working against ITO69. The wavelength this material works well at switching, is relatively long which requires a very high refractive index to compensate. Unfortunately the refractive index of ITO69 at 1.55μm is low further exasperating the confinement problem. This isn't an insurmountable problem if a material can be found with the ability to switch in the infrared range can be found with high refractive index. Experimenting with simulations show that at a refractive index of 5, the confinement is good but there still isn't a good ratio of light in and out of the switch. At a refractive index of 6 this ratio starts looking good. ITO/NbO$_x$ doesn't look like a good fit for building an infrared switch at the 200nm scale, but it does look like it will work for a 200nm scale blue light switch.

Cladding Material Evaluation

Significance: Compare various materials for use in the cladding focusing on refractive index and availability in semiconducting manufacturing.

Method: Literature Review and Simulation

Results:

To create a switch that uses a capacitor as its fundamental structure, dielectric materials must be chosen. These materials were chosen based on their existing association with Si-based fabrication then their refractive indices were compared to the indices of ITO34 and ITO69 to see which would be compatible for both materials. One obvious choice is SiO2 which is the most prevalent dielectric material in the semiconductor industry. In addition to this nanoporous silica, hydrogensilsesquioxanes (HSQ, Teflon-AF (PTFE), silicon oxyflouride (FSG), hafnium silicate (HfSiO$_4$), zirconium silicate (ZrSiO$_4$), and barium titanate (BaTiO$_3$) where looked at [78, 79]. This list was narrowed down based on searching for the approximate refractive index. Materials with refractive indices lower than SiO$_2$ were looked for. It should be noted that most references to refractive index for these materials are

reported as a constant and no wavelength is given for the stated index resulting in some sources reporting seemingly conflicting numbers. Looking at various materials in reference [74] shows that most materials have a significant dependence on wavelength with the general shape of the index showing a spike at short wavelengths and then a somewhat exponentially decreasing curve towards longer wavelengths. Knowing that total internal reflection must be satisfied helped reduce the list of materials to those with refractive indices lower than ITO69 at 1.55µm. This narrowed things down to three: SiO_2, Teflon-AF 1601, and nanoporous silica.

Dielectric Material	n(475nm)	n(1.55µm)
SiO_2	1.4638	1.444
Teflon-AF 1601	1.31	1.295
Nanoporous Silica	1.22	1.20

Table 10. Cladding material refractive indices [80, 81, 82].

The simulations in this section use a 200nm by 200nm structure for ITO34 and a 0.5µm by 1µm structure for ITO69. While the reason for this is apparent from the baseline simulations run on ITO69, it should also be noted that the simulation will not actually run for ITO69 at the 200nm scale because the refractive indices are too close together. The simulation just errors out. At the large scale, the simulations will run. Also the bottom substrate material is always chosen to be SiO_2 for ITO34 to evaluate its compatibility to be just put on top of a wafer using SiO_2 for all of its electrical layers. This was not done on ITO69 because that material even at 0.5µm has issues with how far down the electric field penetrates. With the extremely week index contrast between ITO69 and SiO2 (1.4521 and 1.444 respectively), this will only get worse. This material would absolutely need a barrier layer between it and the rest of the wafer.

Simulations of ITO34 on a SiO₂ substrate and a dielectric of SiO₂, Teflon-AF 1601, and finally

nanoporous silica:
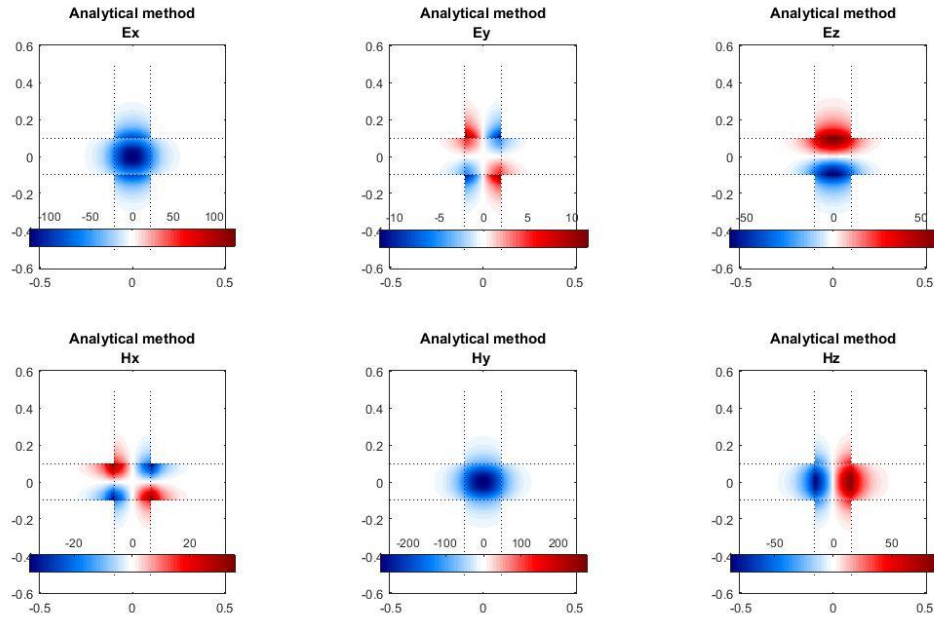
Figure 43. ITO34/SiO₂ at 475nm (x and y axes are in μm)

Field (y-axis)	Limit	10%
E_x	163nm	93nm
E_y	138nm	n/a
E_z	168nm	58nm

Table 11. Field reach from the edge of the light guide in y-axis for ITO34/SiO₂

Field (x-axis)	Limit	10%
E_x	193nm	123nm
E_y	93nm	n/a
E_z	218nm	98nm

Table 12. Field reach from the edge of the light guide in x-axis for ITO34/SiO₂
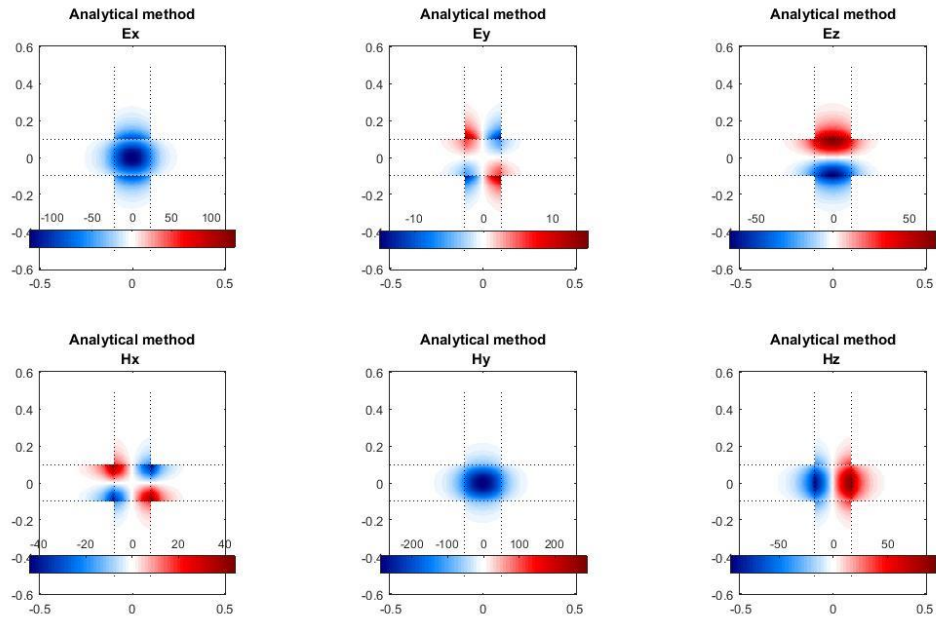
Figure 44. ITO34/Teflon-AF 1601 at 475nm (x and y axes are in μm)

Field (y-axis)	Limit	10%
E_x	163nm	93nm
E_y	128nm	n/a
E_z	168nm	63nm

Table 13. Field reach from the edge of the light guide in y-axis for ITO34/Teflon-AF 1601

Field (x-axis)	Limit	10%
E_x	178nm	113nm
E_y	198nm	8nm
E_z	203nm	93nm

Table 14. Field reach from the edge of the light guide in x-axis for ITO34/Teflon-AF 1601
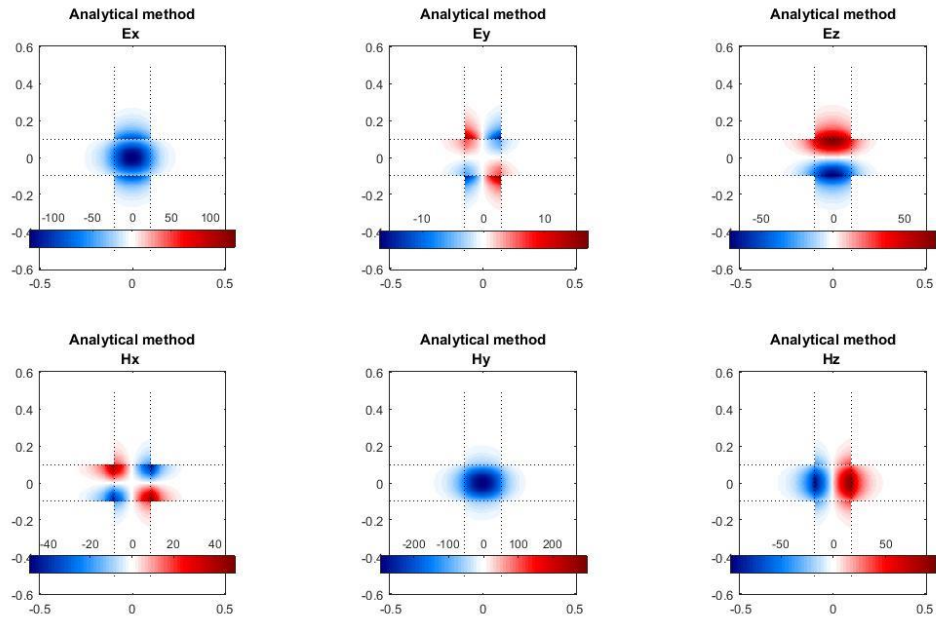
Figure 45. ITO34/nanoporous silica at 475nm (x and y axes are in μm)

Field (y-axis)	Limit	10%
E_x	127nm	93nm
E_y	127nm	n/a
E_z	182nm	68nm

Table 15. Field reach from the edge of the light guide in y-axis for ITO34/nanoporous silica

Field (x-axis)	Limit	10%
E_x	163nm	107nm
E_y	183nm	13nm
E_z	192nm	93nm

Table 16. Field reach from the edge of the light guide in x-axis for ITO34/nanoporous silica

Simulations of ITO69 totally surrounded by dielectric of SiO_2, Teflon-AF 1601, and nanoporous silica.

Note SiO_2 is not used as a substrate for ITO69 because of its poor performance.
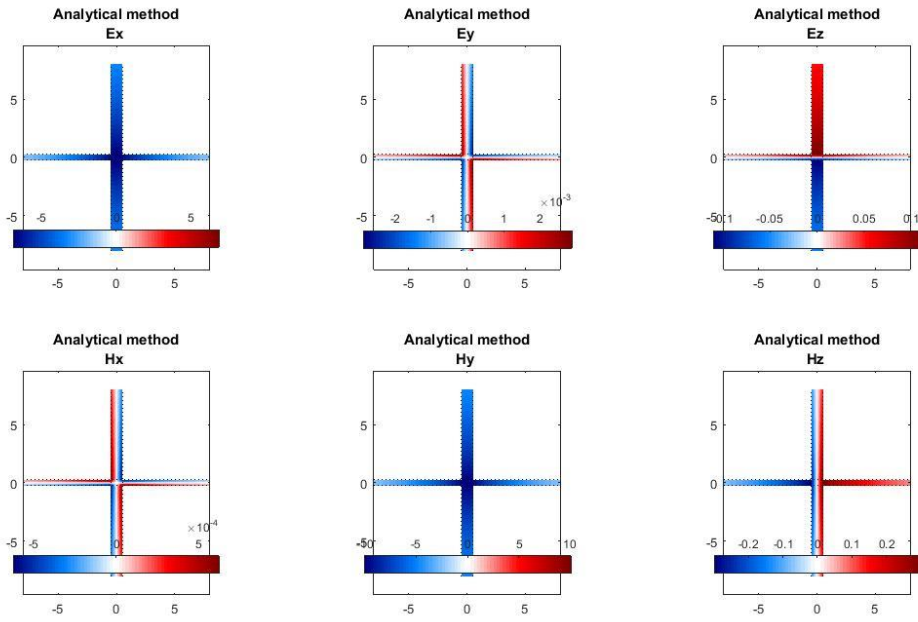
Figure 46. ITO69/SiO$_2$ at 1.55μm (x and y axes are in μm)

Field (y-axis)	Limit	10%
E$_x$	> 8000nm	> 8000nm
E$_y$	> 8000nm	n/a
E$_z$	> 8000nm	n/a

Table 17. Field reach from the edge of the light guide in y-axis for ITO69/SiO$_2$

Field (x-axis)	Limit	10%
E$_x$	> 8000nm	> 8000nm
E$_y$	> 8000nm	n/a
E$_z$	> 8000nm	n/a

Table 18. Field reach from the edge of the light guide in x-axis for ITO69/SiO$_2$
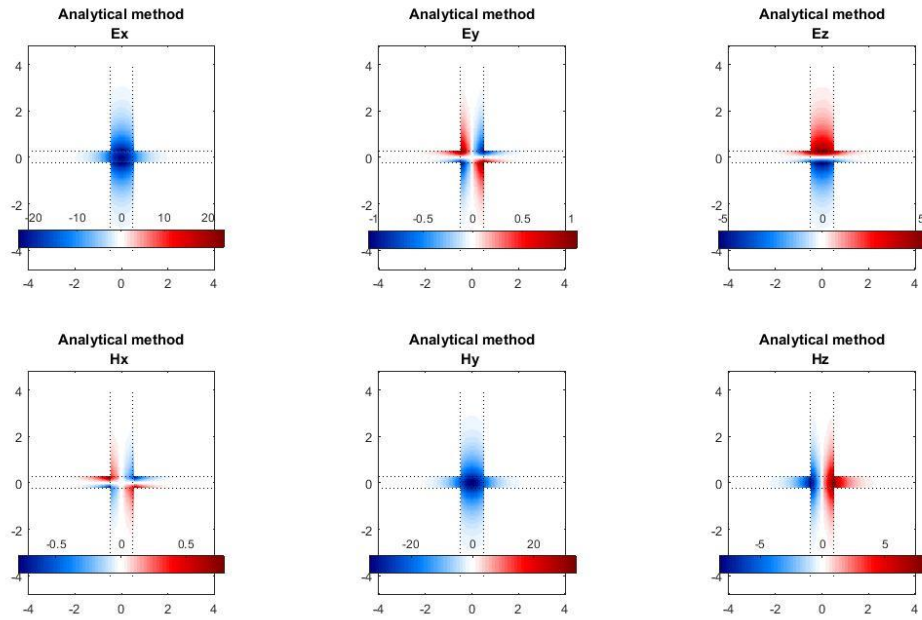
Figure 47. ITO69/Teflon-AF 1601 at 1.55µm (x and y axes are in µm)

Field (y-axis)	Limit	10%
E_x	1500nm	900nm
E_y	1500nm	n/a
E_z	1500nm	300nm

Table 19. Field reach from the edge of the light guide in y-axis for ITO69/Teflon-AF 1601

Field (x-axis)	Limit	10%
E_x	2800nm	1900nm
E_y	2750nm	n/a
E_z	2750nm	700nm

Table 20. Field reach from the edge of the light guide in x-axis for ITO69/Teflon-AF 1601
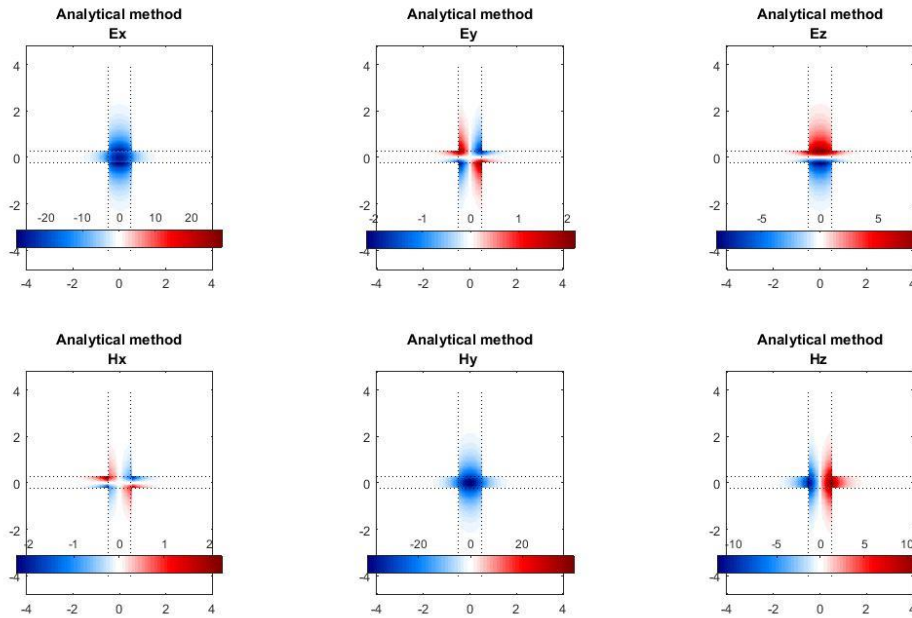
Figure 48. ITO69/nanoporous silica at 1.55µm (x and y axes are in µm)

Field (y-axis)	Limit	10%
E_x	1000nm	650nm
E_y	1150nm	n/a
E_z	1100nm	350nm

Table 21. Field reach from the edge of the light guide in y-axis for ITO69/nanoporous silica

Field (x-axis)	Limit	10%
E_x	2100nm	1200nm
E_y	1750nm	n/a
E_z	1750nm	750nm

Table 22. Field reach from the edge of the light guide in x-axis for ITO69/nanoporous silica

ITO34 shows very good results with good light confinement for all three materials. Since the performance of this material with SiO_2 is good it allows the material to be placed directly on wafers using SiO_2 as their dielectric even if a different dielectric is desired for the switches. Adding the dielectric does result in some loss of switch density moving from a minimum of 67.5nm between switches to a minimum of 93nm between switches for all three dielectric materials. ITO69 performed extremely poorly with SiO_2. This means the most common dielectric in semiconductor manufacturing can't be used with this material. The other two dielectric materials simulated didn't perform too

poorly. The minimum distance between switches was 900nm and 650nm for Teflon-AF 1601 and nanoporous silica respectively. Considering the wavelength of 1.55µm, that wasn't too bad. The issue with ITO69 again was the performance in the x-axis (height of the switch). The resulting minimum distance between switches layered on top of one another was 1.9µm and 1.2µm. While increasing the height of the switch allows for better light confinement allowing for some amount of optimization, micrometer scales for thicknesses on wafers is not very practical. Simulations show that ITO34 with all three dielectric materials tested should function well, but ITO69 will only potentially function with Teflon-AF 1601 and nanoporous, but there are questions about how viable even those materials could be.

Manufacturability

Significance: Compare the materials from the core and cladding material evaluation for manufacturability.

Method: Literature review

Results:

The manufacturability of the materials chosen is critical to this thesis. The whole point was to find a process for optical switching that functioned on small enough scales to be added as a 3D integrated circuit on top of an existing Si-based wafer process. Four materials were examined here, ITO/NbO$_x$, SiO$_2$, Teflon-AF1601, and nanoporous silica.

ITO/NbO$_x$ is a material that is synthesized first in solution where ITO nanoparticles between 5nm and 15nm in diameter are linked with hexaniobates forming the material in ITO/NbO$_x$ that is primarily responsible for its effects. This solution is then mixed with decaniobates to the desired ITO concentration where ITO34 is 34% ITO/hexaniobate and 66% decaniobate. The final product of this preparation is an aqueous colloidal solution that can then be deposited with spin coating. The substrate needs to be treated to make it hydrophilic, which in the case of the original study was treating the surface with ultraviolet-ozone. After spin coating, the resulting film needs to be annealed at 400°C for 20 minutes using a rapid thermal annealing furnace at 10°Cs^{-1} (annealing in air is fine) [5].

The simple spin coating deposition is one of the main reasons this material was chosen for this application making it something that can be applied to a wafer easily. SiO_2 is a staple of the semiconductor industry. This can be deposited by chemical vapor deposition using SiH_4 and O_2 in temperatures ranging from 300°C to 500°C at atmospheric pressure [83]. There is a very significant amount of literature written and industry experience regarding this material. This material effective creates the definition of what other materials must do at a minimum. Teflon-AF 1601 is the DuPont-branded name for polytetraflouethylene or PTFE. This material claims to be unique in that it has the lowest refractive index of any polymer [81]. There are three versions of this material where the amount of dioxole monomer is varied (AF 1300, AF1601, AF2400). Deposition was performed using spin coating where the Teflon-AF was diluted in FC-40 surfactant. The refractive indices for all three versions are relatively close to one another differing by only about 0.015. Since the data showed that thinner films were possible at slower spinning speeds for Telfon-AF 1601 given the same spinning time, it was chosen for simulations. A speed of 2000rpm for 60s resulted in about a 55nm film thickness whereas Teflon-AF 2400 required 5000rpm for 60s to achieve a 60nm film thickness. The bake temperature for the film was 140°C for 60 seconds [81]. It should be noted that the glass transition temperature for Teflon-AF 2400 is given as 240°C which is well below the 400°C required for annealing ITO/NbO_x. This calls into question how well this material could handle the high temperatures required for this annealing process. Nanoporous silica is a process quite similar to ITO/NbO_x. The chemistry here seeks to create silica nanoparticles suspended in solution using a base process (using TEOS, ethanol, and water). The research showed that although it is possible to produce the material using an acid and two step acid/base process, it was only the sample prepared using the base process that showed the extraordinarily low refractive index [82]. SEM imaging of films made with acid-catalyzed and base-catalyzed nanoporous silica show the base-catalyzed version to have smaller structures showing a dependence of optical performance on the size of the pores. The deposition method for nanoporous silica was dip-coating. The film thickness was controlled by controlling the draw speed of the wafer out of the solution. The silica solution was treated with an ultrasonator for 30 minutes prior to dip deposition to separate unstable aggregate. After coating, the film was placed in an ammonia

atmosphere for 24 hours and then baked at 400°C for 2 hours [82]. This process also places it within the same range of temperatures as the ITO/NbO$_x$ and SiO$_2$.
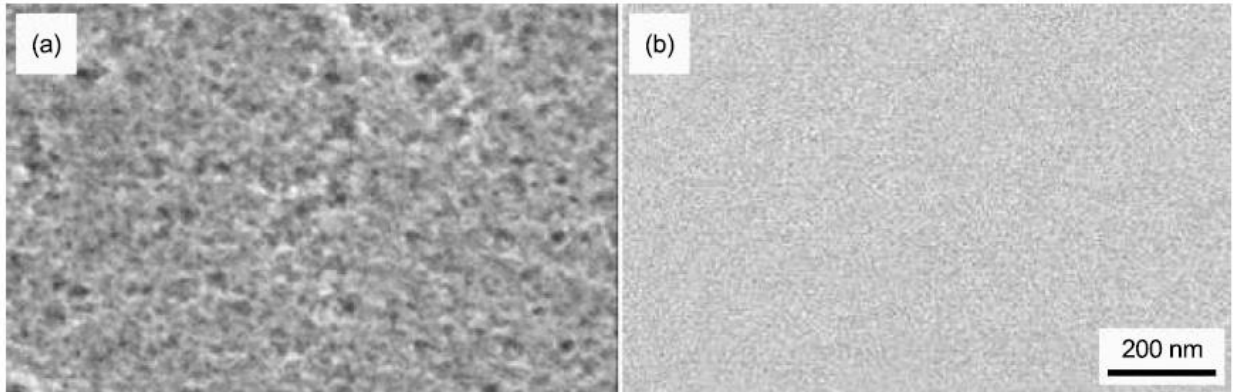
Figure 49. SEM images comparing acid-catalyzed (a) to base-catalyzed (b) nanoporous silica [82]

ITO/NbO$_x$, SiO$_2$, and nanoporous silica all show good compatibility with standard Si-based wafer fabrication. Teflon-AF 1601 raises questions about whether it could actually survive the temperatures required for the ITO/NbO$_x$ and SiO$_2$ (if used again) and whether it would retain all of its properties afterward. Routinely taking the material above the glass transition temperature would also mean the structural integrity of other things like the metal lines might be compromised and potentially put additional stress on the ITO/NbO$_x$ during processing. Given there are alternatives with fewer questions, it is likely SiO$_2$ or nanoporous silica should be considered for the dielectric material.

The following is a process recommendation for the structure of the switch. Note this process doesn't take into consideration light generation or optical/electrical conversion. The dielectric material chosen is SiO$_2$, the metal lines and vias chosen are the Aluminum and Tungsten respectively, and the active layer is ITO/NbO$_x$ (ITO34). For the sake of this example, vias are ignored to focus on building up the actual proposed switch. Additionally, the bottom electrode here is the metal layer and the top electrode is the ITO/NbO$_x$ but it should be noted that there is no reason this must be true. There is nothing preventing the bottom electrode from being the ITO/NbO$_x$ and the top electrode being the metal layer. The intention is for this process to be built up on top of a Si wafer. First a layer of SiO$_2$ is necessary to provide isolation from the lower metal interconnect layers for the Si wafer (note that vias

would obviously be needed in this layer to ensure electrical connections to the Al bottom electrodes. Next the Al metal layer needs to be deposited over the whole wafer (there are established processes for chemical vapor and sputtering deposition for Si wafer processes). After the Al another layer of SiO_2 must be deposited after which the ITO/NbO_x layer must be put down. Then a photo resist needs to be put down to create the pattering for the switches. The next step is to etch all three layers of ITO/NbO_x, SiO_2, and Al to create small capacitors that will function as switches due to the ITO/NbO_x electrode (through which the light will travel). Another layer of SiO_2 needs to be added to fully surround the switches and provide electrical isolation for the conductive layers. The final step needs to be a planarization since the switches are relatively tall and the final SiO_2 layer will likely be quite uneven at the top. At this point another etch process would need to occur to add the necessary vias to create the electrical connections to the ITO/NbO_x top electrodes.

Figure 50. Full stack of ITO/NbO_x, SiO_2, and Al creating the basis for the capacitors/switches
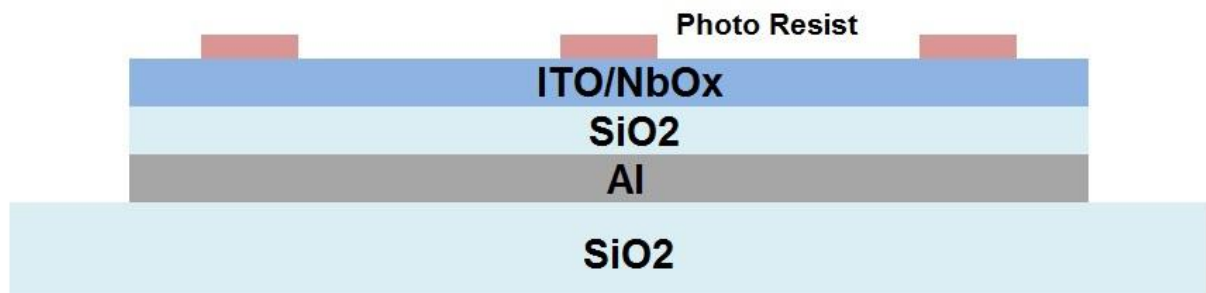
Figure 51. Photo resist to create the actual individual switches
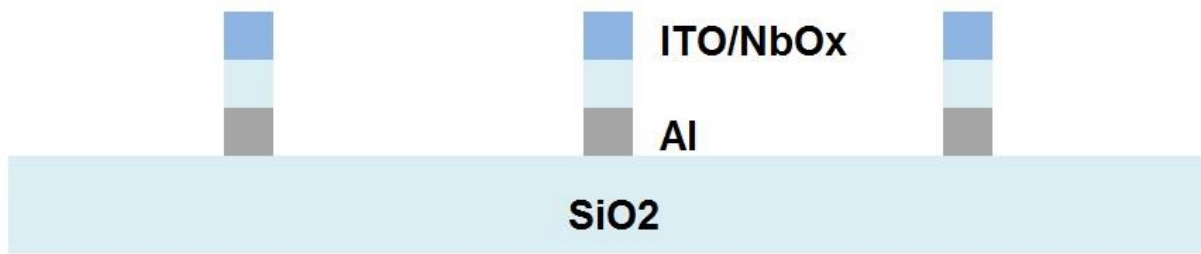
Figure 52. After etching to produce the individual switches
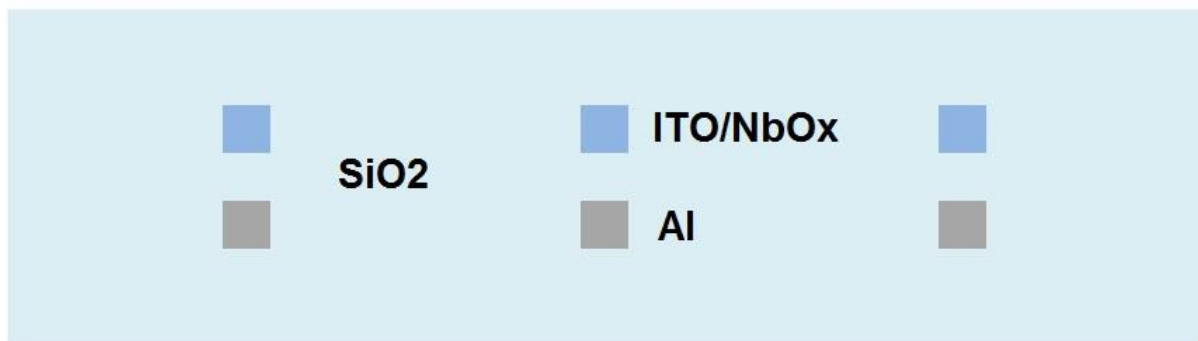
Figure 53. After final SiO₂ deposition and any necessary planarization

The final product will be small capacitors that, in the case of ITO/NbO$_x$, will allow light to pass through the top electrode when charged and will block light when discharged.

CHAPTER 4 FUTURE WORK

This thesis only addresses the idea of an optical switch controlled by an electric field for a specific material: ITO/NbO$_x$. It seeks to evaluate its possible use as an active device that could be fabricated on top of a Si wafer. This is not the only material that could potentially have applications as a switch. There also are a number of problems that fall outside the scope of this initial work. Most notably is the generation and distribution of light and converting that light back to electrical charge that can be deposited onto the switches to turn then on and off. Nor does this thesis address how charge could be bleed off the electrodes in order to switch the other way. ITO/NbO$_x$ was chosen for this work because of its simple deposition method and annealing temperature making it compatible with existing wafer processes. This is a somewhat unique material that has very interesting properties but hasn't been exhaustively researched. The refractive index needs to be experimentally determined not just estimated based on the individual ITO and NbO$_x$ properties. A very important piece of information that needs to be experimentally determined is the isotropicity of the material. Research into thin films examine how light interacts with them in a direction that is actually perpendicular to how it is intended to travel through this switch. The concern here is related to how the light is propagating with respect to the applied electric field that is intended to produce the transmittance change. In the case of this switch the electric field will also be perpendicular to the direction the light is propagating. This is something that needs to be investigated since this is not really a scenario for which there has needed to be much research. While it is reasonable to assume that if the material is isotropic this will not be a concern, it would be wise to consider the light propagation direction and applied electric field direction scenario simply because of a lack of research.

CHAPTER 5 SUMMARY

The goal of this research was to investigate the feasibility of creating an optical switch that would be compatible with Si wafers. The literature review provided a promising material in ITO/NbO$_x$ that showed itself to have potential for use in the short wavelength visible range, specifically 475nm. Unfortunately this material did not show good results for the infrared range due to the poor refractive index at longer wavelengths. A material with a significantly higher refractive index would be necessary to provide good light confinement. The 475nm simulations showed good results with SiO$_2$ showing that switches with sizes similar to late 1990s Si transistor node sizes. A 100nm process would be needed to produce switches placed 100nm apart and 200nm wide and could use industry established processes for metallization, SiO$_2$ deposition and ITO/NbO$_x$ deposition (spin coating/annealing). While there is nothing stopping the simulations from going to smaller sizes, it is likely that much below 200nm widths would result in problems getting consistent performance from switch to switch due to the use of ITO nanoparticles in ITO/NbO$_x$. This research provides the ground work developing a voltage controlled optical switch that could be placed onto Si wafers to build a 3D integrated circuit without the need of additional wafers or through-Si vias.

BIBLIOGRAPHY

BIBLIOGRAPHY

[1]   Roland Lenz. "Introduction to all optical switching technologies." Available:
        http://imedea.uib-
        csic.es/~salvador/coms_optiques/addicional/tutorials/intro_allopticalswitching.pdf, Jan. 30,
        2003 [Accessed Aug. 12, 2015].

[2]   I. Glaser. "Lenslet array processors." *Applied Optics*, Vol 21, Issue 7, pp. 1271-1280, 1982
        doi: 10.1364/AO.21.001271

[3]   Usman Pirzada. "Intel ISSCC: 14nm all figured out, 10nm is on track, Moores Law still alive and
        kicking." Internet: http://wccftech.com/intel-isscc-14nm/. WCCF Tech. July 2, 2015.

[4]   Parthiban Santhanam, Dodd Joseph Gray, Jr., and Rajeev J. Ram. "Thermoelectrically Pumped
        Light-Emitting Diodes Operating above Unity Efficiency." *Physical Review Letters*, Vol 108,
        Issue 6, 097403. Feb 27, 2012.
        http://journals.aps.org/prl/abstract/10.1103/PhysRevLett.108.097403

[5]   Anna Llordés, Guillermo Garcia, Jaume Gazquez, and Delia J. Milliron. "Tunable near-infrared
        and visible-light transmittance in nanocrystal-in-glass composites." *Nature*, Vol 500, pp 323-
        326, Aug 15, 2013.
        doi: 10.1038/nature12398

[6]   Pierre Ambs. "Optical Computing: A 60-Year Adventure." *Advances in Optical Technologies*, Vol
        2010, Article ID 372652, Feb 19, 2010
        doi: 10.1155/372652

[7]   Optalysys company website [Online]. Available: http://optalysys.com/technology/ [Accessed
        April 11, 2017].

[8]   M. Fernando Gonzalez-Zalba, Sergey N. Shevchenko, Sylvain Barraud, J. Robert Johansson,
        Andrew J. Ferguson, Franco Nori, and Andreas C. Betz. "Gate-Sensing Coherent Charge
        Oscillations in a Silicon Field-Effect Transistor." *Nano Letters*, Vol 2016, pp 1614-1619, Feb 11,
        2016.
        doi: 10.1021/acs.nanolett.5b04356

[9]   M. Veldhorst, C. H. Yang, J. C. C. Hwang, W. Huang, J. P. Dehollain, J. T. Muhonen, S.
        Simmons, A. Laucht, F. E. Hudson, K. M. Itoh, A. Morello, A. S. Dzurak. "A two-qubit logic gate
        in silicon." *Nature*, Vol 526, pp 410-414, October 15, 2015.
        dio: 10.1038/nature15263

[10]   S. Debnath, N. M. Linke, C. Figgatt, K. A. Landsman, K. Wright, and C. Monroe. "Demonstration
        of a small programmable quantum computer with atomic qubits." *Nature*, Vol 536, pp 63-66,
        Aug 4, 2016.
        dio: 10.1038/nature18648

[11]   D. Hillerkuss, R. Schmogrow, T. Schellinger, M. Jordan, M. Winter, G. Huber, T. Vallaitis, R.
        Bonk, P. Kleinow, F. Frey, M. Roeger, S. Koenig, A. Ludwig, A. Marculescu, J. Li, M. Hoh, M.
        Dreschmann, J. Meyer, S. Ben Ezra, N. Narkiss, B. Nebendahl, F. Parmigiani, P. Petropoulos, B.
        Resan, A. Oehler, K. Weingarten, T. Ellermeyer, J. Lutz, M. Moeller, M. Huebner, J. Becker, C.
        Koos, W. Freude and J. Leuthold. "26 Tbit s[-1] line-rate super-channel transmission
        utilizing all-optical fast Fourier transform processing." *Nature Photonics*, Vol 5, pp 364-371,
        May 22, 2011.
        dio: 10.1038/NPHOTON.2011.74, Alternate

[12]   S. A. Hamilton*, Member, IEEE* and B. S. Robinson*, Student Member, IEEE*. "40-Gb/s All-Optical Packet Synchronization and Address Comparison for OTDM Networks." *IEEE Photonics Technology Letters*, Vol. 14, No. 2, pp 209-211, Feb 2002.
dio: 10.1109/68.980524

[13]   A.J. Poustie, K.J. Blow 1, A.E. Kelly, and R.J. Manning. "All-optical full adder with bit-differential delay." *Optical Communications*, Vol 168, pp 89-93, Sept 1, 1999.
dio: 10.1016/S0030-4018(99)00348-X

[14]   Francisco M. Raymo and Massimiliano Tomasulo. "Optical Processing with Photochromic Switches." *Chemistry European Journal*, 12, pp 3186-3193, Jan 17, 2006.
dio: 10.1002/chem.200501178

[15]   Ramaswami, Rajiv, Kumar Sivarajan, and Galen Sasaki. *Optical networks: a practical perspective*. Morgan Kaufmann, 2009.

[16]   Batya Feldman. "Optical processing co Lenslet closes" [Online]. Available: http://www.globes.co.il/en/article-1000067464. March 2, 2006 [Accessed April 10, 2017].

[17]   "EnLight256® 8000 Giga MAC / sec fixed point DSP." Available: http://besho.narod.ru/reviews/newage/EnLight256.pdf. 2003 [Accessed April 10, 2017]

[18]   D. Hisamoto, Wen-Chin Lee, J. Kedzierski, E. Anderson, H. Takeuchi, K. Asano, Tsu-Jae King, J. Bokor, and Chenming Hu. "A Folded-channel MOSFET for Deep-sub-tenth Micron Era." *IEDM Tech. Dig 1998*, pp 1032-1034, Dec, 1998.
dio: 10.1109/IEDM.1998.746531

[19]   Arabinda Das and Alexandre Dorofeev. "Intel's 22-nm process gives MOSFET switch a facelift" [Online]. Sept 6,2012 [Accessed April 10, 2017].

[20]   J. M. Early. "Speed, power and component density in multielement high-speed logic systems." *1960 International Solid-State Circuits Conference*, pp 78-79, March 1960.
dio: 10.1109/ISSCC.1960.1157266

[21]   Paul D. Franzon, W. Rhett Davis, Michael B. Steer, Steve Lipa, Eun Chu Oh, Thor Thorolfsson, Samson Melamed, Sonali Luniya, Tad Doxsee, Stephen Berkeley, Ben Shani, and Kurt Obermiller. "Design and CAD for 3D Integrated Circuits." *Proceedings of the 45th annual Design Automation Conference*, pp 668-673, June 8, 2008.
dio: 10.1145/1391469.1391642

[22]   Cristinel Ababei, Yan Feng, Brent Goplen, Hushrav Mogal, Tianpei Zhang, Kia Bazargan, and Sachin S. Sapatnekar. "Placement and Routing in 3D Integrated Circuits." *IEEE Design & Test of Computers*, pp 520-531, Volume: 22, Issue: 6, Nov.-Dec. 2005.
dio: 10.1109/MDT.2005.150

[23]   Rafael Reif, Andy Fan, Kuan-Neng Chen, and Shamik Das. "Fabrication Technologies for Three-Dimensional Integrated Circuits." *Quality Electronic Design, 2002. Proceedings. International Symposium on*, Aug 7, 2002.
dio: 10.1109/ISQED.2002.996687

[24]   A. W. Topol, D. C. La Tulipe, Jr., L. Shi, D. J. Frank, K. Bernstein, S. E. Steen, A. Kumar, G. U. Singco, A. M. Young, K. W. Guarini, and M. Ieong. "Three-dimensional integrated circuits." *IBM Journal of Research and Development*, Vol 50, No. 4.55, pp 491-506, July, 2006.
dio: 10.1147/rd.504.0491

[25]   "What is 3D Integration?" [Online]. Available: http://www.3dincites.com/3d-incites-knowledge-portal/what-is-3d-integration/. [Accessed Oct 2, 2016].

[26]   Steven M. Pope, and Ruben C, Zeta (Maxim Integrated Products, Inc.). "Package-on-Package Secure Module Having Anti-Temper Mesh in the Substrate of the Upper Package." U.S. Patent 7 923 830 B2, April 12, 2011.
Alt: 7 923 830 B2

[27]   Robert S. Patti. "Three-Dimensional Integrated Circuits and the Future of System-on-Chip Designs." *Proceedings of the IEEE*, Vol 94, Issue 6, pp 1214-1224, June, 2006.
dio: 10.1109/JPROC.2006.873612

[28]   Rachel Courtland. "The Rise of the Monolithic 3-D Chip." *IEEE Spectrum,* [Online]. Available: http://spectrum.ieee.org/semiconductors/design/the-rise-of-the-monolithic-3d-chip/. Feb 24th, 2014 [Accessed Oct 4, 2016].

[29]   Anna Llordés, Guillermo Garcia, Jaume Gazquez, and Delia J. Milliron. "Tunable near-infrared and visible-light transmittance in nanocrystal-in-glass composites." *Nature*, Vol 500, pp 323-326, Aug 15, 2013.
dio: 10.1038/nature12398

[30]   Christoforos Kachris, Ioannis Tomkos. "A Survey on Optical Interconnects for Data Centers." *IEEE Communications Surveys and Tutorials*, Vol 14, No. 4, pp 1021-1036, Jan 11th, 2012.
dio: 10.1109/SURV.2011.122111.00069

[31]   Xiaohua Ma, Geng-Sheng (G. S.) Kuo. "Optical switching technology comparison: optical MEMS vs. other technologies." *IEEE Communications Magazine*, Vol 41, Issue 11, Nov, 2003.
dio: 10.1109/MCOM.2003.1244924

[32]   Mitsunori Saito, Aki Maruyama, and Junki Fujiwara. "Polarization-independent refractive-index change of a cholesteric liquid crystal." *Optical Materials Express*, Vol 5, Issue 7, pp 1588-1597, June 12, 2015.
dio: 10.1364/OME.5.001588

[33]   Shi-Sheng Lee, Long-Sun Huang, Chang-Jin Kim, and Ming C. Wu. "Free-Space Fiber-Optic Switches Based on MEMS Vertical Torsion Mirrors." *Journal of Lightwave Technology*, Vol 17, No. 1, pp 7-13, Jan, 1999.
dio: 10.1109/50.737414

[34]   Hsin-ta Hsieh, Chen-wei Chiu, Tom Tsao, Fukang Jiang, and Guo-Dung John Su. "Low-Actuation-Voltage MEMS for 2-D Optical Switches." *Journal of Lightwave Technology*, Vol 24, No. 11, pp 4372-4379, Nov, 2006.
dio: 10.1109/JLT.2006.883674

[35]   Yao-Joe Yang, Bo-Ting Liao and Wen-Cheng Kuo. "A novel 2 × 2 MEMS optical switch using the split cross-bar design." *Journal of Micromechanics and Microengineering*, Vol 17, No. 5, April 3rd, 2007.
dio: 10.1088/0960-1317

[36]   Pierre-Alexandre Blanche, Daniel Carothers, John Wissinger, and Nasser Peyghambarian. "Digital micromirror device as a diffractive reconfigurable optical switch for telecommunication." *Special Section On Emerging MOEMS Technology And Applications*, Vol 13, Issue 1, Dec 2nd, 2013.
dio: 10.1117/1.JMM.13.1.011104

[37]   Arash Joushaghani, Brett A. Kruger, Suzanne Paradis, David Alain, J. Stewart Aitchison, and
        Joyce K. S. Poon. "Low-voltage broadband hybrid plasmonic-vanadium dioxide switches."
        Applied Physic Letters, Volume 102, Issue 6, Feb, 2013.
        dio: 10.1063/1.4790834

[38]   Xiaofang Yu, and Shanhui Fan, "Bends and splitters for self-collimated beams in photonic
        crystals." *Applied Physic Letters*, Volume 83, Issue 16, Oct, 2003.
        dio: 10.1063/1.1621736

[39]   Yuanliang Zhang, Yao Zhang, and Baojun Li. "Optical switches and logic gates based on self-
        collimated beams in two-dimensional photonic crystals." *Optics Express*, Vol. 15, Issue 15, pp
        9287-9292, July 13, 2007.
        dio: 10.1364/OE.15.009287

[40]   Photonic Crystals, Theory, Applications and Fabrication, Page 11.

[41]   Hannes Kind, Haoquan Yan, Benjamin Messer, Matthew Law, and Peidong Yang. "Nanowire
        Ultraviolet Photodetectors and Optical Switches." *Advanced Materials*, Vol. 14, Issue 2, pp 158-
        160, Jan 16, 2002.
        dio: 10.1002/1521-4095(20020116)14:23.0.CO;2-W

[42]   Jianfang Wang, Mark S. Gudiksen, Xiangfeng Duan, Yi Cui, and Charles M. Lieber. "Highly
        Polarized Photoluminescence and Photodetection from Single Indium Phosphide Nanowires."
        Science, Vol. 293, Issue 5534, pp 1455-1457, Aug 24, 2001.
        dio: 10.1126/science.1062340

[43]   Roman Bruck, and Otto L. Muskens. "Plasmonic nanoantennas as integrated coherent perfect
        absorbers on SOI waveguides for modulators and all-optical switches." *Optics Express*, Vol. 21,
        Issue 23, pp 27652-27661, Nov 4, 2013.
        dio: 10.1364/OE.21.027652

[44]   K. Lance Kelly, Eduardo Coronado, Lin Lin Zhao , and George C. Schatz. "The Optical Properties
        of Metal Nanoparticles: The Influence of Size, Shape, and Dielectric Environment." *Journal of
        Physical Chemistry B*, Vol. 107, Issue 3, pp 668–677, Dec 21, 2002.
        dio: 10.1021/jp026731y

[45]   E. Prodan, C. Radloff, N. J. Halas, P. Nordlander. "A Hybridization Model for the Plasmon
        Response of Complex Nanostructures." *Science*, Vol. 302, Issue 5644, pp. 419-422, Oct 17,
        2003.
        dio: 10.1126/science.1089171

[46]   Iván O. Sosa, Cecila Noguez, and Rubén G. Barrera. "Optical Properties of Metal Nanoparticles
        with Arbitrary Shapes." *Journal of Physical Chemistry B*, Vol. 107, Issue 26, pp 6269–6275, June
        7, 2003.
        dio: 10.1021/jp0274076

[47]   W. Rechberger, A. Hohenau, A. Leitner, J.R. Krenn, B. Lamprecht, and F.R. Aussenegg.
        "Optical properties of two interacting gold nanoparticles." *Optics Communications*, Vol. 220,
        pp 137-141, March 17, 2003.
        dio: 10.1016/S0030-4018(03)01357-9

[48]   Emilie Ringe, Richard P Van Duyne, and Laurence D Marks. "Correlated structure-optical
        properties studies of plasmonic nanoparticles." *Journal of Physics: Conference Series*, Vol. 522,
        conference 1, 2014.
        dio: 10.1088/1742-6596/522/1/012006

[49]   Yu Zhang, Alejandro Manjavacas, Nathaniel J. Hogan, Linan Zhou, Ciceron Ayala-Orozco, Liangliang Dong, Jared K. Day, Peter Nordlander, and Naomi J. Halas. "Toward Surface Plasmon-Enhanced Optical Parametric Amplification (SPOPA) with Engineered Nanoparticles: A Nanoscale Tunable Infrared Source." *Nano Letters*, Vol. 16, Issue 5, pp 3373-3378, April 18, 2016.
          dio: 10.1021/acs.nanolett.6b01095

[50]   Jacob A. Faucheaux, Alexandria L. D. Stanton, and Prashant K. Jain. "Plasmon Resonances of Semiconductor Nanocrystals: Physical Principles and New Opportunities." *Journal of Physical Chemistry Letters*, Vol. 5, Issue 6, pp 976-985, Feb 27, 2014.
          dio: 10.1021/jz500037k

[51]   G A Niklasson1, S-Y Li and C G Granqvist. "Thermochromic vanadium oxide thin films: Electronic and optical properties." *Journal of Physics: Conference Series*, Vol. 559, conference 1, 2014.
          dio: 10.1088/1742-6596/559/1/012001

[52]   Shuyan Zhang, Mikhail A. Kats, Yanjie Cui, You Zhou, Yu Yao, Shriram Ramanathan, and Federico Capasso. "Current-modulated optical properties of vanadium dioxide thin films." *Applied Physics Letters*, Vol. 105, Issue 21, Nov, 2014.
          dio: 10.1063/1.4902924

[53]   J.-C. Orlianges, J. Leroy, A. Crunteanu, R. Mayet, P. Carles, and C. Champeaux. "Electrical and optical properties of vanadium dioxide containing gold nanoparticles deposited by pulsed laser deposition." *Applied Physics Letters*, Vol. 101, Issue 13, Sept, 2012.
          dio: 10.1063/1.4754708

[54]   Kannatassen Appavoo, Bin Wang, Nathaniel F. Brady, Minah Seo, Joyeeta Nag, Rohit P. Prasankumar, David J. Hilton, Sokrates T. Pantelides, and Richard F. HaglundJr. "Ultrafast Phase Transition via Catastrophic Phonon Collapse Driven by Plasmonic Hot-Electron Injection." *Nano Letters*, Vol. 14, Issue 3, pp 1127-1133, Jan 31, 2014.
          dio: 10.1021/nl4044828

[55]   R Maiti, A Midya, C Narayana, and S K Ray. "Tunable optical properties of graphene oxide by tailoring the oxygen functionalities using infrared irradiation." *Nanotechnology*, Vol. 25, Issue 49, Nov 21, 2014.
          dio: 10.1088/0957-4484/25/49/495704

[56]   Alexander I. Chernov, Pavel V. Fedotov, Alexandr V. Talyzin, Inma Suarez Lopez, Ilya V. Anoshkin, Albert G. Nasibulin, Esko I. Kauppinen, and Elena D. Obraztsova. "Optical Properties of Graphene Nanoribbons Encapsulated in Single-Walled Carbon Nanotubes." *American Chemical Society Nano*, Vol. 7, Issue 7, pp 6346-6353, June 24, 2013.
          dio: 10.1021/nn4024152

[57]   A. V. Kretinin, Y. Cao, J. S. Tu, G. L. Yu, R. Jalil, K. S. Novoselov, S. J. Haigh, A. Gholinia, A. Mishchenko, M. Lozada, T. Georgiou, C. R. Woods, F. Withers, P. Blake, G. Eda, A. Wirsig, C. Hucho, K. Watanabe, T. Taniguchi, A. K. Geim, and R. V. Gorbachev. "Electronic Properties of Graphene Encapsulated with Different Two-Dimensional Atomic Crystals." *Nano Letters*, Vol. 14, Issue 6, pp 3270-3276, May 20, 2014.
          dio: 10.1021/nl5006542

[58]   Hao Wang, Hua Zhao, Guangwei Hu, Siren Li, Hang Su, and Jingwen Zhang. "Graphene Based Surface Plasmon Polariton Modulator Controlled by Ferroelectric Domains in Lithium Niobate." *Scientific Reports*, Vol. 5, Article Num. 18258, Dec 14, 2015.
          dio: 10.1038/srep18258

[59]   Qiuyun Ouyang, Hailong Yu, Zheng Xu, Yue Zhang, Chunyan Li, Lihong Qi, and Yujin Chen. "Synthesis and enhanced nonlinear optical properties of graphene/CdS organic glass." *Applied Physics Letters*, Vol. 102, Issue 3, Jan, 2013.
         dio: 10.1063/1.4789367

[60]   Andrea Ambrosini, Angel Duarte, Kenneth R. Poeppelmeier, Melissa Lane, Carl R. Kannewurf, Thomas O. Mason. "Electrical, Optical, and Structural Properties of Tin-Doped In2O3+M2O3 Solid Solutions (M 5Y, Sc).", *Journal of Solid State Chemistry*, Vol. 153, Issue 1, pp 41-47, Aug, 2000.
         dio: 10.1006/jssc.2000.8737

[61]   Sok Won, Kim; Manil, Kang; Inkoo, Kim; Minwoo, Chu; Ji-Wook, Ryu. "Optical Properties of Sputtered Indium-tin-oxide Thin Films." *Journal of the Korean Physical Society*, Vol. 59, Issue 51, pp 3280-3283, April 30, 2011.
         dio: 10.3938/jkps.59.3280

[62]   Michael Gross, Albrecht Winnacker, and Peter J. Wellmann. "Electrical, optical and morphological properties of nanoparticle indium–tin–oxide layers." *Thin Solid Films*, Vol. 515, Issue 24, pp 8567-8572, Oct 15, 2007.
         dio: 10.1016/j.tsf.2007.03.136

[63]   J Ederth, P Heszler, A Hultåker, G.A Niklasson, and C.G Granqvist. "Indium tin oxide films made from nanoparticles: models for the optical and electrical properties." *Thin Solid Films*, Vol 445, Issue 2, pp 199-206, Dec 15, 2003.
         dio: 10.1016/S0040-6090(03)01164-7

[64]   Sebastien D. Lounis, Evan L. Runnerstrom, Amy Bergerud, Dennis Nordlund, and Delia J. Milliron. "Influence of Dopant Distribution on the Plasmonic Properties of Indium Tin Oxide Nanocrystals." *Journal of the American Chemical Society*, Vol. 136, Issue 19, pp 7110-7116, April 30, 2014.
         dio: 10.1021/ja502541z

[65]   Limin Tong, Jingyi Lou, and Eric Mazur. "Single-mode guiding properties of subwavelength-diameter silica and silicon wire waveguides." *Optics Express*, Vol. 12, Issue 6, pp 1025-1035, March 9, 2004.
         dio: 10.1364/OPEX.12.001025

[66]   Robert Halir, Przemek J. Bock, Pavel Cheben, Alejandro Ortega-Moñux, Carlos Alonso-Ramos, Jens H. Schmid, Jean Lapointe, Dan-Xia Xu, J. Gonzalo Wangüemert-Pérez, Íñigo Molina-Fernández, and Siegfried Janz. "Waveguide sub-wavelength structures: a review of principles and applications." *Laser and Photonics Reviews*, Vol. 9, Issue 1, pp 25-49, Sept 30, 2014.
         dio: 10.1002/lpor.201400083

[67]   Richard Feynman. "QED: Fits of Reflection and Transmission -- Quantum Behaviour", *The Sir Douglas Robb Lectures*, University of Auckland, 1979.

[68]   Junjie Du, Shiyang Liu, Zhifang Lin, Jian Zi, and S. T. Chui. "Dielectric-based extremely-low-loss subwavelength-light transport at the nanoscale: An alternative to surface-plasmon-mediated waveguiding." *Physical Review A*, Vol. 83, Issue 3, March 14, 2011.
         dio: 10.1103/PhysRevA.83.035803

[69]   Yin Huang, Changjun Min, and Georgios Veronis. "Subwavelength slow-light waveguides based on a plasmonic analogue of electromagnetically induced transparency." *Applied Physics Letters*, Vol. 99, Issue 14, Oct 7, 2011.
         dio: 10.1063/1.3647951

[70]   Jennifer M. Reed, Haining Wang, Yingnan Guo, and Shengli Zou. "Subwavelength light confinement and propagation: A numerical study of a two-layer silver film with perforated holes." *Applied Physics Letters*, Vol. 103, Issue 16, Oct 17, 2013.
dio: 10.1063/1.4826441

[71]   Aristeidis Karalis, J. D. Joannopoulos, and Marin Soljačić. "Plasmonic-Dielectric Systems for High-Order Dispersionless Slow or Stopped Subwavelength Light." *Physical Review Letters*, Vol. 103, Issue 4, July 24, 2009.
dio: 10.1103/PhysRevLett.103.043906

[72]   Seunghoon Han, Yi Xiong, Dentcho Genov, Zhaowei Liu, Guy Bartal, and Xiang Zhang. "Ray Optics at a Deep-Subwavelength Scale: A Transformation Optics Approach." *Nano Letters*, Vol. 8, Issue 12, pp 4243-4247, Oct 29, 2008.
dio: 10.1021/nl801942

[73]   R. Quidant, J.-C. Weeber, A. Dereux, D. Peyrade, Y. Chen, and C. Girard. "Near-field observation of evanescent light wave coupling in subwavelength optical waveguides." *Europhysics Letters*, Vol. 57, Issue 2, pp 191-197, 2002.
dio: 10.1209/epl/i2002-00560-3

[74]   "Refractive Index of ITO, Indium Tin Oxide, InSnO" [Online]. Available: http://www.filmetrics.com/refractive-index-database/ITO/Indium-Tin-%20Oxide-InSnO. [Accessed April 8, 2017].

[75]   M. Baum, I. Alexeev, M. Latzel, S. H. Christiansen, and M. Schmidt. "Determination of the effective refractive index of nanoparticulate ITO layers." *Optics Express*, Vol 21, Issue 19, pp 22754, Sept 23, 2013.
dio: 10.1364/OE.21.022754

[76]   "Optical constants of Nb2O5 (Niobium pentoxide)" [Online]. Available: https://refractiveindex.info/?shelf=main&book=Nb2O5&page=Lemarchand. [Accessed April 8, 2017].

[77]   Wouter J. Westerveld, Suzanne M. Leinders, Koen W. A. van Dongen, H. Paul Urbach, and Mirvais Yousefi. "Extension of Marcatili's Analytical Approach for Rectangular Silicon Optical Waveguides." *Journal of Lightwave Technology*, Vol. 30, Issue 14, pp 2388-2401, July 15, 2012.
dio: 10.1109/JLT2012.2199464

[78]   "Dielectric Materials" [Online]. Available: https://www.gelest.com/applications/dielectric-materials/. [Accessed April 8, 2017].

[79]   "Dielectric materials for semiconductor chips" [Online]. Available: http://www.eeherald.com/section/design-guide/dielectric_in_semiconductors.html. Accessed April 8, 2017].

[80]   "Refractive Index of SiO2, Fused Silica, Silica, Silicon Dioxide, Thermal Oxide, ThermalOxide" [Online]. Available: http://www.filmetrics.com/refractive-index-database/SiO2/Fused-Silica-Silicon-Dioxide-Thermal-Oxide-ThermalOxide. [Accessed April 8, 2017].

[81]   Min K. Yang, Roger H. French, and Edward W. Tokarsky. "Optical properties of Teflon® AF amorphous fluoropolymers." *Journal of Micro/Nanolithography, MEMS, and MOEMS*, Vol 7, Issue 3, Aug 13, 2008.
dio: 10.1117/1.2965541

[82]   Yiqun XIAO, Jun SHENy, Zhiyong XIE, Bin ZHOU and Guangming WU. "Microstructure Control of Nanoporous Silica Thin Film Prepared by Sol-gel Process." *Journal of Materials Science and Technology*, Vol 23, Issue 4, pp 504-508, Aug 27, 2007.
dio: 10.3321/j.issn:1005-0302.2007.04.014

[83]   John Foggaito. "Chemical Vapor Deposition of Silicon Dioxide Films." *Handbook of Thin Film Deposition*, Chapter 3, pp 120, 2001.
Available online: https://booksite.elsevier.com/9781437778731/
https://booksite.elsevier.com/9781437778731/past_edition_chapters/Chemical_Vapor.pdf